ORIGINAL PAPER

Assessment of seismic hazard including equivalent-linear soil response analysis for Dhaka Metropolitan Region, Bangladesh

Masoud Mojarab[1] · Nazi Norouzi[1] · Mahdokht Bayati[1] · Zeinab Asadi[1] ·
Mohamad Eslami[1] · Mohsen Ghafory-Ashtiany[2] · Abdul-Latif Helaly[3] ·
Sara Khoshnevis[4]

Abstract

Dhaka is one of the most populated cities in the world, which means that the occurrence of natural hazards will put the city in a critical situation. A seismic hazard analysis (SHA) is a prerequisite to reduce the risk of an earthquake event in Dhaka. This paper, focusing on the active faults of Bangladesh and the soil condition, represents the calculation of the peak ground acceleration (PGA), spectral acceleration (SA), and amplification factor. The analysis here used an updated seismic catalog (up to 2020), three source models (linear, areal, and smoothed seismicity), and eight attenuation models (selected by ranking techniques). Data from drillings are used to build the soil model, and one-dimensional frequency-domain equivalent-linear analysis is applied to calculate the amplification factor and the acceleration on the surface. The results show that the PGA changes from 0.14 to 0.19 and from 0.33 to 0.46 on bedrock for a return period of 475 and 2475 years, respectively. The worst-case scenario for Dhaka is the movement of the Jamuna Fault (Madhapur section), which can cause a PGA from 0.08 to 0.68 on bedrock. The results also suggest that the soil can amplify the acceleration up to 2.4 times. PGA on the surface for the return period of 475 years varies from 0.18 to 0.41. The design spectra and zonation maps are presented in the paper.

✉ Masoud Mojarab
mmojarab@gmail.com

1   Bonyan Zamin Paydar Consulting Engineers, Tehran, Iran

2   International Institute of Earthquake Engineering and Seismology, Tajrish, Iran

3   Rajdhani Unnayan Kartripakkha, Urban Resilience Project, Dhaka, Bangladesh

4   Protek-Yapi Consulting Engineers, Istanbul, Turkey

1 Introduction

Bangladesh is a part of the Himalayan foredeep and the down-wrapped Bengal Basin. After the complete subduction of the Tethys oceanic crust between India and Eurasia, it became an interaction between two continental plates, which sutured themselves together to form a larger continent (Gupta 2006). In 1993, the Bangladesh National Building Code (BNBC) provided the seismic hazard zoning map to determine the minimum design earthquake forces for buildings. Bangladesh has been divided into three seismic zones based on seismic ground motion with a 2% probability of exceedance within 50 years (Ministry of Housing & Public Works 1993). In the latest revision of BNBC, the seismic classification of Bangladesh is changed from three to four zones (Ministry of Housing & Public Works 2020).

Zhang et al. (1999) developed the PGA hazard map with a 10% probability of exceedance in 50 years for continental Asia as part of the Global Seismic Hazard Assessment Program. Al-Hussaini and Al-Noman (2010) computed probabilistic seismic hazard for Bangladesh using different attenuation relationships and delineation of seven seismic sources. Kolathayar et al. (2012) and Nath and Thingbaijam (2012) estimated seismic hazards for India and adjoining areas using deterministic and probabilistic approaches, respectively. Also, the Global Earthquake Model (GEM) in Global Seismic Hazard Map developed the distribution of the PGA for the return period of 475 years computed for seismic rock conditions (V_{S30} = 760–800 m/s) using the OpenQuake engine (Pagani et al. 2018). Mase et al. 2021 provided a comprehensive seismic hazard vulnerability based on a probabilistic approach in Bengkulu City, Indonesia, which is recommended in its seismic design code. The results show that PGA in Bengkulu City ranges from 0.2 to 0.5 g. SA at 0.2 s and 1 s ranges from 0.4 to 1.3 g and 0.4 to 0.7 g, respectively.

Furthermore, Haque et al. (2019) assessed the probabilistic seismic hazard by modifying seismic sources in Bangladesh. In this work, the spectral acceleration for 2% and 10% probabilities of exceedance in 50 years has been calculated using OpenQuake by considering the site effects. More recently, Rahman et al. (2020) performed a probabilistic seismic hazard analysis (PSHA) for Bangladesh. They prepared the PGA and spectral acceleration (periods of 0.2, 0.5, 1.0, 2.0, 5.0, and 10.0 s) maps at the bedrock for both return periods of 475 and 2475 years.

In the present study, PSHA has been conducted for the DMR, considering uncertainties by applying the logic tree approach. SHA relies on seismotectonic interpretations, identification of seismic sources, earthquake catalog development, and selection of GMPEs to estimate the probability of ground motion at a given level at a specific site. Here, the OpenQuake engine has been used. The OpenQuake engine has been introduced by Pagani et al. (2014), and since then, many researchers around the world used this platform for seismic hazard and risk assessment (Yilmaz et al. 2021; Du and Pan 2020; Zimmaro and Stewart 2017; Villar-Vega et al. 2017; Chaulagain et al. 2015).

2 SHA on bedrock

Various approaches are available for SHA. Each one of these approaches can be performed in detail by studying seismotectonic, identification of faults, developing a homogenous earthquake catalog, delineation of seismic sources, and selecting proper GMPEs. In the

current work, SHA has been performed using GEM's OpenQuake based on classical PSHA (for various return periods of 50, 75, 100, 200, 475, 2475, and 10,000 years) and scenario-based approaches.

2.1 Regional tectonic of Bangladesh

The Bengal Basin results from the collision of the Indian Shield with the Eurasian Plate in the north and the collision with the Burma Plate in the east. The Himalaya is a consequence of the collision of the Eurasian and Indian Plates about 50 Ma (Valdiya 1984). The Indian Plate is subducting along the Sunda and Andaman trenches with a highly oblique convergence (Satyabala 2003; Stork et al. 2008; Hurukawa et al. 2012). The predominant tectonic regime in this region is compression with the northward motion of the Indian Plate relative to the Eurasian Plate at a rate of ~ 18–20 cm/yr (Kumar et al. 2007). According to Socquet et al. (2006), the relative movement between the India and Sunda Plates is 35 mm/yr. The strike-slip motion between the India and Sunda Plates, along the Sagaing Fault, accommodates displacement at a rate of 18 mm/yr. Mallick et al. (2019) inferred active convergence across the Indo-Barman ranges at a rate of ~ 12–24 mm/year.

2.2 Earthquake catalog, magnitude homogenization, and declustering

Compiling a uniform earthquake catalog is a critical tool in SHA. Figure 1 shows the reviewed existing catalogs for the subject region.

A primary concern for investigating historical seismicity is how they are assembled. The reliability of historical catalogs varies considerably over time, and it can be very low for the early period. Most of the historical earthquake catalogs, probably due to insufficient observation or macroseismic data, are not complete or homogeneously compiled in terms of epicentral locations and magnitude. To prioritize the various historical seismic databases and selection of historical earthquakes among available databanks, some criteria and related rating classes have been defined according to the quality and quantity of intensity observations as presented in Table 1.

Fig. 1 The timeline of existing earthquake databases (Pandey et al. 2017; Nath et al. 2017b; Alam and Dominey-Howes 2016; Kolathayar et al. 2012; Martin and Szeliga 2010; Szeliga et al. 2010; Kayal 2008b; Ambraseys and Douglas 2004)

Table 1 The defined reliability criteria for historical seismic data

Rating class		Description of reliability criteria
A	–	Existence of excellent or reassessed isoseismal maps
	–	Existence of sufficient intensity observations for the approximation of epicentral location and magnitude
B	–	Events that have been reported by more than two databases
C	–	Events that have been reported by just one database
	–	Existence of insufficient intensity observations
	–	Epicentral location approximation is based on poor evidence

According to the defined reliability criteria, Ambraseys and Douglas (2004) and Szeliga et al. (2010) have the highest priority due to the reassessment of isoseismal maps and approximation of earthquake epicenter location by more than five intensity observations, respectively. However, the events with lower rating classes were conservatively selected in the list of historical earthquakes.

For instrumental earthquakes, besides available international catalogs such as ISC, the catalogs provided by Nath et al. (2017b), Kolathayar et al. (2012), Alam and Dominey-Howes (2016), and Pandey et al. (2017) can be applied. Due to differences in the coverage area of various catalogs, a rectangular region bounded by latitudes 17.8° N–29.5° N and longitudes 83.4° E–97.5° E that cover the radius of 300 km from DMR has been selected for further investigations.

First of all, duplicated data have been removed by setting the proximity limits of the temporal, location, and magnitude differences. After that, to select the most accurate and complete earthquake database, the area and period of coverage, homogeneity, completeness, continuity of events, the number of events, and variation of earthquake magnitude and depth through time for each catalog were investigated aiming to compare the various earthquake databanks. Finally, the catalog developed by Nath et al. (2017b) has been selected for further investigation. Nath et al. (2017b) compiled an earthquake catalog for the period of 1900–2014. To complete the catalog from 2014 to 2017/12/1 and from 2017/12/1 to 2020/02/28, the seismic events extracted from the Reviewed ISC Bulletin and USGS are added to the catalog, respectively.

A homogeneous earthquake catalog with a uniform magnitude scale is an important part of SHA. Figure 2 compares the trend lines of empirical relations for converting surface and body wave magnitudes to moment magnitude developed by Nath et al. (2017b), Kolathayar et al. (2012), Pandey et al. (2017), Das et al. (2011), Yadav et al. (2010), and Scordilis (2006). By applying the log-likelihood (LLH) methodology, the relation of Nath et al. (2017b) has been selected for the homogeneity of the earthquake catalog.

It is necessary to have a catalog with Poisson's behavior. For each earthquake catalog, the subsequent shocks are identified as aftershocks if they occur within a specified time and distance interval (van Stiphout et al. 2012). In the present project, the Gardner and Knopoff (1974) algorithm has been applied for declustering.

Finally, a homogeneous earthquake catalog has been compiled within a radius of 300 km from DMR containing historical and instrumental events. Historical earthquakes were extracted from databases provided by Ambraseys and Douglas (2004), Szeliga et al. (2010), Kolathayar et al. (2012), and Alam and Dominey-Howes (2016), respectively. The distribution of the declustered earthquake catalog is shown in Fig. 3.
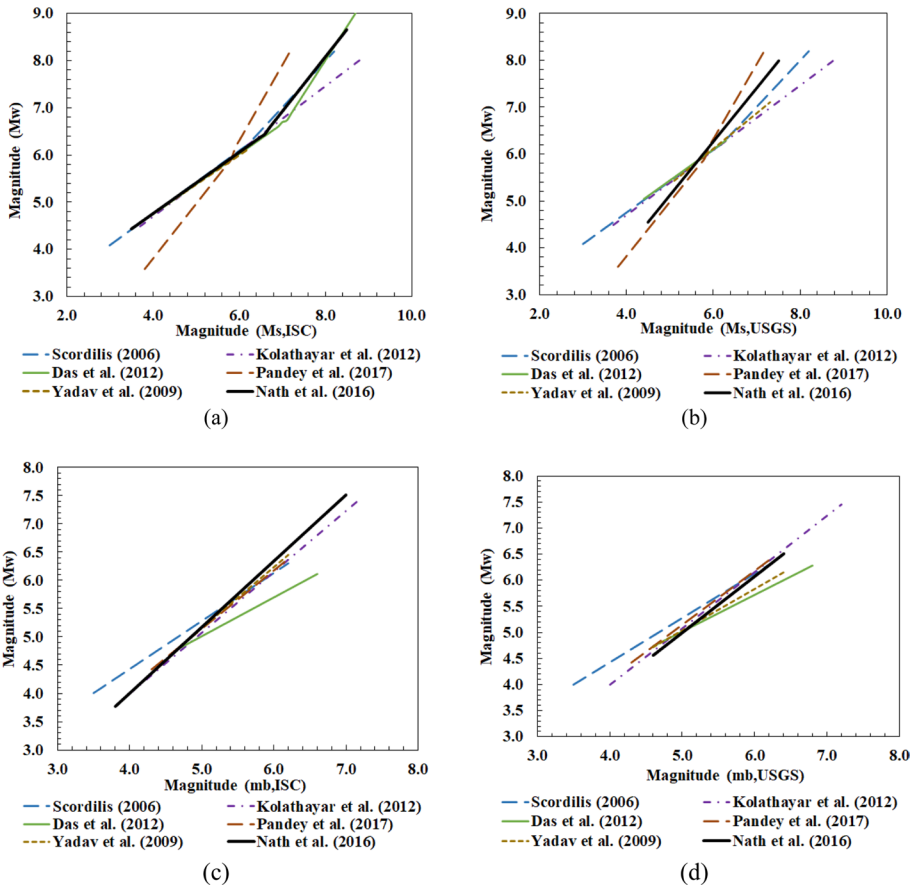
Fig. 2 Comparison of the empirical relations for converting magnitudes **a** MS, ISC-MW, **b** MS, USGS-MW **c** mb, ISC-MW, and **d** mb, USGS-MW

Also, the magnitude histogram, time histogram, and variation of earthquake magnitude versus time for the final catalog are shown in Fig. 4.

2.3 Seismic source determination

Three types of sources are identified here to conduct the SHA. Areal sources are areas with the same seismicity pattern and behavior (McGuire 2004). In this research, seven areal sources in the study area are identified.

Source A: Combining seismic density and topography of the Dauki Fault zone, the border of source A is defined. The eastern boundary of zone A is recognized by the Dhubri lineament. A significant point in this seismic zone is its excellent compatibility with the gravity anomaly map. The zone is also well aligned with the Shillong Massif state of Bangladesh tectonic map.
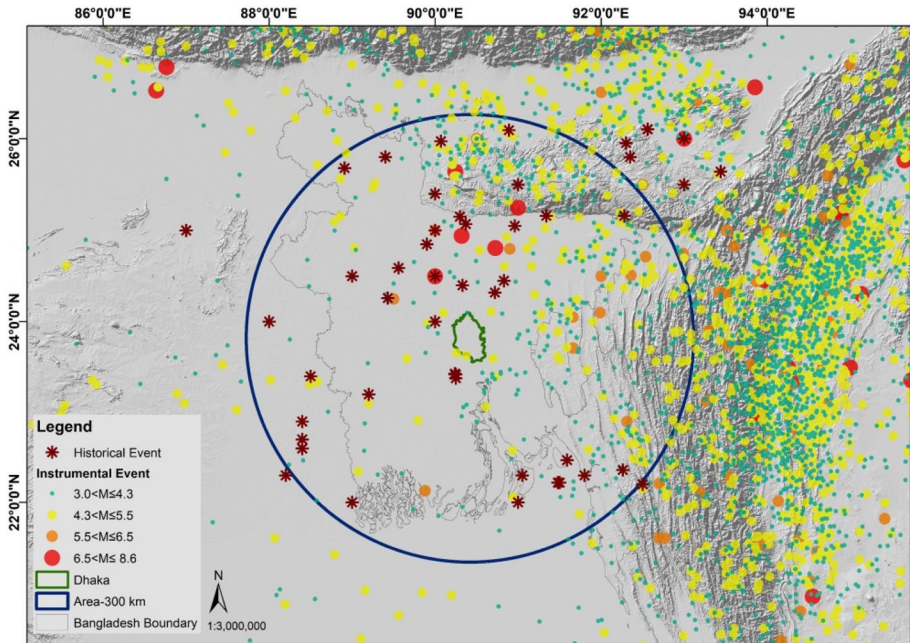
Fig. 3 Distribution of earthquake catalog within the radius of 300 km from Dhaka

Source B: This seismic source is located in the shallow crust subduction transition zone. The Chittagong Coastal Fault (CCF) and the Kaladan Fault are assumed as the eastern and western borders of this source. From the west to the east, the morphology is slightly changing from flat plain to slightly folded and finally to completely folded. It can be divided into two sources. Sources B1 and B2 are located just in contact with the slightly folded zone and completely folded zone. These zones are in good consistent with the gravity anomaly and the tectonic map of Bangladesh. Seismicity is increasing from west to east, and the depth of earthquakes increases just after seismic sources B1 and B2. The border between seismic zones B1 and B2 has been identified based on the Kaladan Fault.

Source C: This source is also divided into two parts. The seismic sources C1 and C2 are located in the west of Dhaka and contain two tectonic zones of Bangladesh. These zones have very low seismicity compared to their neighboring seismic sources. A remarkable point in these sources is their very high correlation with the gravity map. C1 is limited to the Dauki Fault and Dhubri lineament in the north. The map of seismic sources provided by Kolathayar et al. (2012) was used to determine the western boundaries of these zones and the southern border of C2.

Source D: Source D is located between B1 and C2, in an area with differences in gravity and magnetic anomaly. It has low seismicity in general, but the distribution of historical earthquakes is significant. There is a complete alignment of this source with the tectonic map of Bangladesh. The eastern boundary of the source is distinguished by the northeast–southwest lineaments. This zone includes Dhaka City and is highly effective. The lower boundary of this
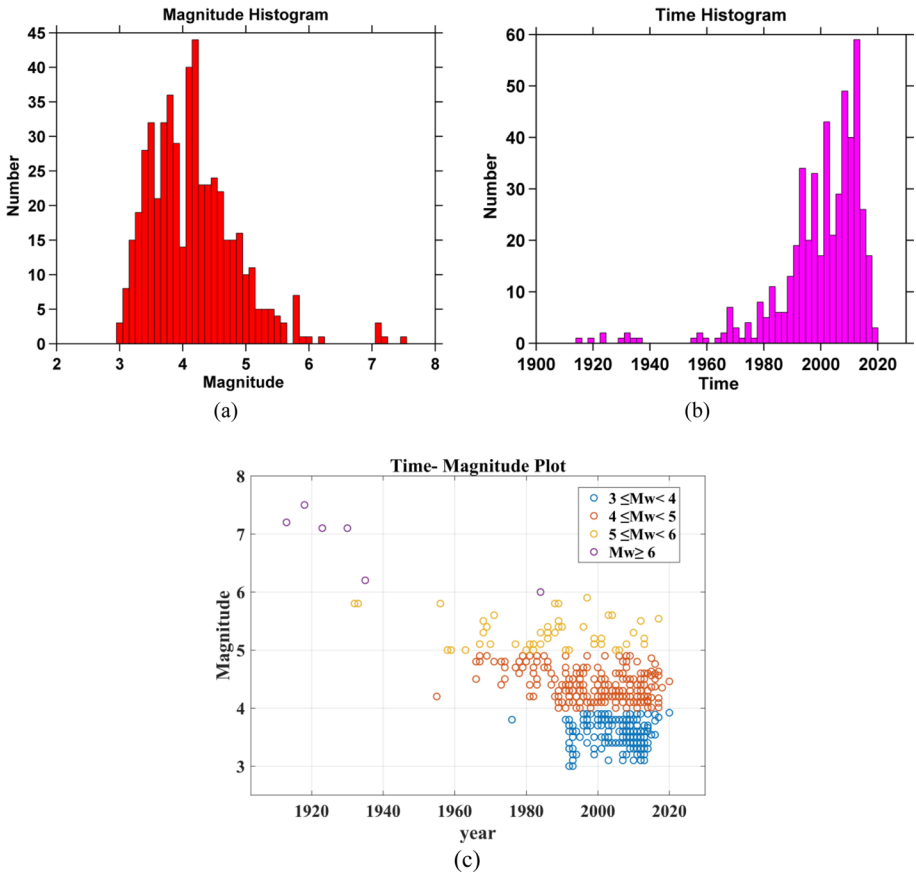
Fig. 4 Magnitude **a** and time **b** histogram of final instrumental catalog, and variation of magnitude through the time **c**

seismic source ends at the seismic source zones provided by Kolathayar et al. (2012).

Source E: It is located between B1 and D, in full compliance with the tectonic map of Bangladesh. This zone is determined and limited by significant faults and lineaments. The lower boundary of this source ends at the boundaries of seismic sources provided by Kolathayar et al. (2012). In terms of seismicity, this source is located in a transition zone between the low and high seismicity of the collision zone.

The design of an area source requires activity rates and nodal plane distribution. The focal mechanism or the fault plane solution of earthquakes that have been reported by various agencies was used to define earthquake ruptures that are consistent with the area source and the tectonic feature (Fig. 5).

In this study, the faults are presented as linear sources due to their separable activity. Faults are defined as narrow zones due to the depth of the seismogenic layer and the fault's dip. To recognize and investigate the faults maps with different scales, GeoEye satellite
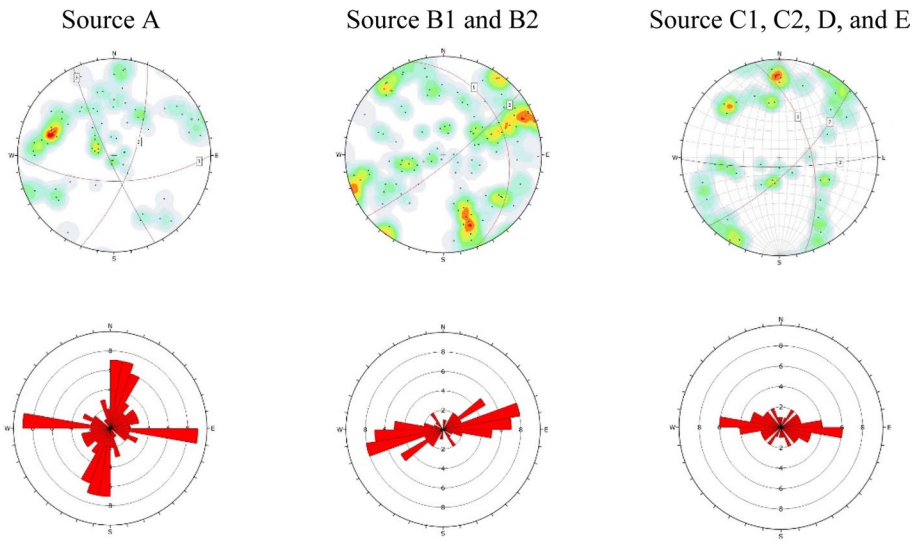
Source A   Source B1 and B2   Source C1, C2, D, and E

Fig. 5 Nodal plane distribution consistent with areal sources

images, SRTM images, Google Earth images, magnetic, gravity, and more importantly, the published papers on active faults in the study area are used. The structural geology elements within the 300-km radius of DMR are represented in Table 2.

One problem is that earthquake catalogs generally include large quantities of events, which do not seem to be linked to any fault, and the reliability of parameters can be questionable (Ouillon et al. 2008). The 3D geometry of faults might lead to a better definition seismogenic potential of the source by constraining the maximum area that can be ruptured by the earthquake (Boncio et al. 2004). In this paper, a multi-objective fuzzy particle swarm optimization algorithm is used to assign earthquakes to each fault and increase the reliability of the catalog. The maximum depth of events is employed to limit the depth of faults, and with the dip angle, a 3D plane is defined for each fault. In this algorithm, the 3D Euclidean distance of each event from each fault plane and the 3D Euclidean distance of each event from each cluster centroid are minimized (Ghasemi Nejad et al. 2021).

As a result, it was found that with the Dauki Fault, the effect of the Oldham and Dapsi Faults can be overlooked. These two faults decrease the impact of the Dauki Fault in SHA. Therefore, they are removed from the list of linear sources. The rest of the faults are separated and identified in the implemented clustering model, and the earthquakes are assigned to them. Figure 6 shows the results of running the algorithm. It is visible in Fig. 6 (a) that there are two specified areas with no faults. Area 1 corresponds to the identified location of the Sylhet lineament, and it can be considered and investigated as a probably blind fault. Likewise, the Paoma lineament (Fig. 6—area 2) was added to the linear seismic sources. Figure 6 (b) shows the final result with all the linear sources and events assigned to them. Table 3 gives the list of these linear sources with their mechanism, dip direction, and total length used in this paper. Table 3 also presents the list of "observed" earthquakes assigned to the mentioned faults based on the literature review.

Another source that is considered here is smoothed seismicity. The idea of the smoothed seismicity maps was introduced by Frankel (1995) to get away from the judgments involved in drawing seismic source zones. This approach relies on dividing the area of interest into

Table 2 Structural geology elements within the 300-km radius of DMR

No.	Name	Mechanism	Dip direction	Reference
1	Dauki Fault	Thrust	N	(Alam et al. 2003; Kayal 2008b; Gahalaut and Kundu 2012; Islam and Shinjo 2012; Morino et al. 2014; Mallick et al. 2019)
2	Dapsi Thrust	Thrust	NE	(Raoof et al. 2017)
3	Dhubri Fault	Lineament	-	(Raoof et al. 2017)
4	Sylhet	Lineament	-	(Islam and Shinjo 2012; Raoof et al. 2017)
5	CCF	Thrust	E	(Gahalaut and Kundu 2012; Hurukawa et al. 2012; Morino et al. 2014)
6	Jamuna Fault	Thrust	NEE	(Morino et al. 2014; Raoof et al. 2017)
7	Paoma	Lineament	-	(Kayal 2008b; Raoof et al. 2017)
8	Tista	Lineament	-	(Kayal 2008b; Islam and Shinjo 2012; Raoof et al. 2017)
9	Oldham Fault	Thrust	NE	(Islam and Shinjo 2012)
10	Kaladan Fault	Thrust	E	(Alam et al. 2003; Gahalaut and Kundu 2012; Hurukawa et al. 2012; Raoof et al. 2017)
11	L1	Lineament	-	(Raoof et al. 2017)
12	L 2	Lineament	-	(Raoof et al. 2017)

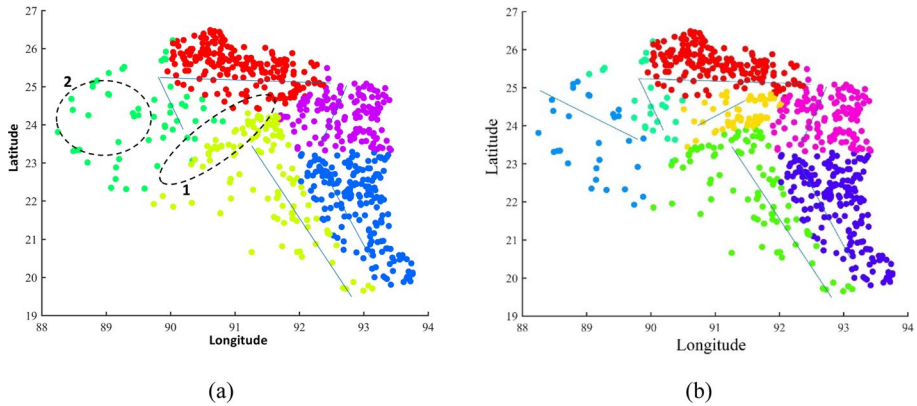(a)   (b)

Fig. 6 Assigning earthquakes using the clustering algorithm

a grid of cells. Each cell is characterized by the cumulative number of earthquakes (n_i) for Mw ≥ Mc, where i is the cell index. The grid of n_i values is then smoothed spatially by multiplying by a Gaussian function with correlation distance (Frankel 1995). In this paper, to define smoothed seismicity, earthquakes with magnitude equal to or greater than Mw 4.0 from 1964 to February 2020 have been used.

Earthquake frequency for cells has been determined on a grid around the study area. Dimensions of each cell vary from 0.1 to 0.5. It has been expected that the distribution of the earthquakes follows Gutenberg–Richter scattering with a b-value equal to what has been estimated in related areal sources of each node. Finally, the rate for each grid cell has been computed. Grid nodes have been smoothed by applying a Gaussian kernel between neighboring cells with a variable correlation distance of 50, 100, and 150. The annual occurrence rate distributions estimated from the various depth, grid spacing, and correlation distances are shown in Fig. 7. Finally, the grided a-value spaced at increments of 0.1° with a correlation distance of 50 km has been selected (Fig. 8).

2.4 Earthquake catalog completeness

The magnitude of completeness (Mc) is the lowest magnitude at which the maximum frequency of magnitude has occurred (Rydelek and Sacks 1989). It will change spatially and temporally because of the increase in the number of seismographs in the region. In this paper, the Mc for each linear and areal seismic source has been determined by the frequency–magnitude distribution (Fig. 9), which was suggested by Wiemer and Wyss (2000).

2.5 Seismicity parameters evaluation

The seismicity parameters have been computed employing the maximum-likelihood procedure provided by Kijko and Sellevoll (1992) and Kijko (2004) and Gutenberg and Richter (1944) recurrence relation. The estimated seismicity parameters are presented in Table 4, and the variation of a-value and b-value calculation based on mentioned procedures is provided in Fig. 10.

Table 3 List of linear sources

Name	Mechanism	Dip direction	Total length (km)	Observed earthquake (Ref.)
Dauki	Thrust	N	300	AD 840–920; 1548; 1897 (Mw: 8) (Islam and Shinjo 2012; Raoof et al. 2017; Morino et al. 2014) AD 1400–1470, 1664 (Mw: 7.8) (Morino et al. 2014) 645–980 AD; 535–530 BC; 810–400 BC (Rajendran et al. 2004) 1950 (Islam and Shinjo 2012; Raoof et al. 2017) 1923/9/9 (Mw: 7); 1930/7/2 (Mw: 7.1) (Kayal 2008b)
CCF	Thrust	E	550	1762/4/2 (Mw: 6.3) AD 680 to 980 BC 150 to AD 60 BC 1395 to 740(Kamal 2013)
Jamuna	Thrust	NEE	175	(Kamal 2013)
Kaladan	Thrust	E	520	-
Sylhet	Lineament	-	160	Before the sixteenth century (Kamal 2013) 1918/07/08 (Mw: 7.1) (Kayal 2008b; Islam et al. 2011; Raoof et al. 2017)
Paoma	Lineament	-	210	-

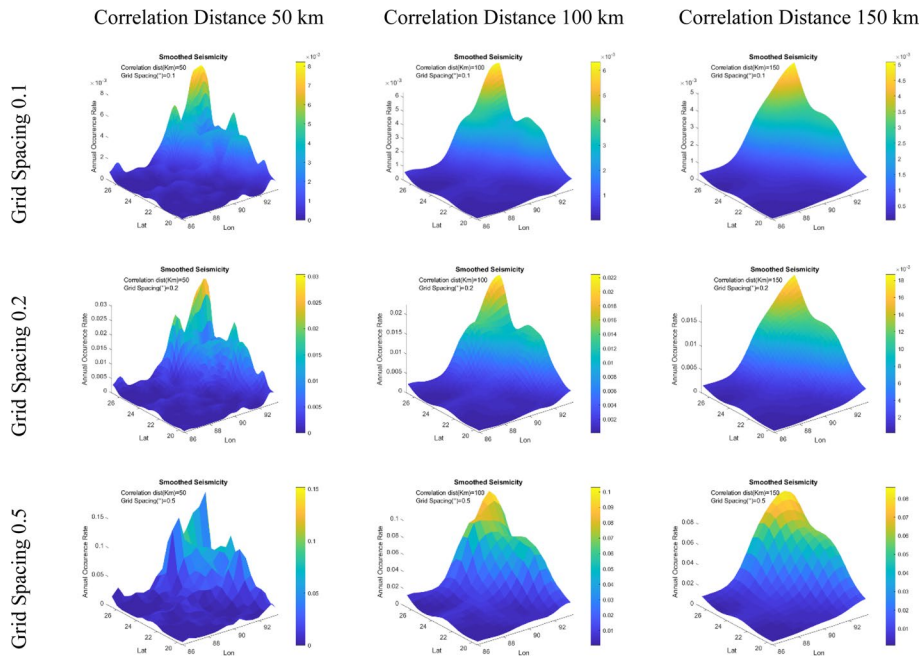**Fig. 7** Smoothed seismicity map, for grid spacing 0.1°, 0.2°, 0.5°, and the correlation distance 50, 100, and 150 km
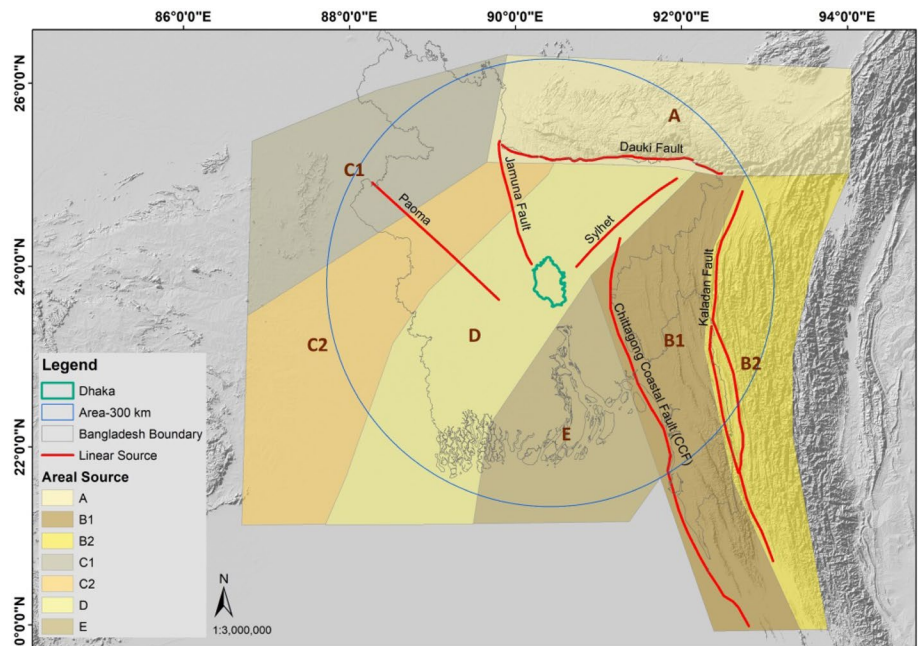

Fig. 8 Areal and linear seismic sources used in the present analysis

Fig. 9 Cumulative and noncu-
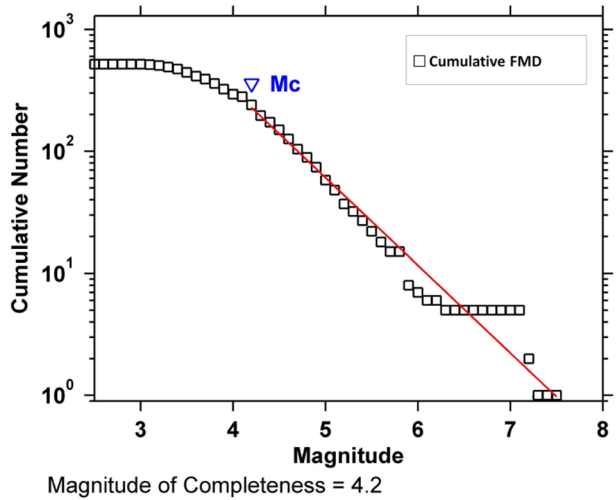mulative frequency–magnitude
distribution

Magnitude of Completeness = 4.2

Table 4 The estimated seismicity parameters

Seismic source model		Mc	(Kijko and Sellevoll 1992) & (Kijko 2004)					(Gutenberg and Richter 1944)	
			M_{max}	Lambda	Beta	a- value	b- value	a- value	b- value
Areal source	A	4.2	6.3	3.50	2.48	3.77	1.08	4.35	0.95
	B1	3.8	6.0	1.24	1.64	2.48	0.71	2.59	0.66
	B2	4.3	6.4	1.69	1.93	2.69	0.84	3.51	0.76
	C1	4.1	6.4	1.07	2.14	2.75	0.93	1.34	0.78
	C2	4.1	6.4	1.36	2.14	2.87	0.93	1.70	0.78
	D	3.9	6.0	1.07	1.61	2.27	0.70	2.56	0.66
	E	3.7	6.4	1.11	1.91	2.05	0.83	2.70	0.72
Linear source	Dauki	4.2	8.0	0.94	1.88	2.41	0.82	2.97	0.72
	Sylhet	3.9	6.1	0.38	1.51	2.11	0.66	1.95	0.61
	CCF	3.8	6.0	0.92	2.01	2.07	0.87	2.98	0.79
	Jamuna	4.1	7.7	0.10	1.35	2.04	0.59	1.23	0.55
	Paoma	4.2	6.7	0.19	2.42	1.98	1.05	3.22	0.94
	Kaladan	4.4	6.4	1.77	2.15	2.58	0.93	3.96	0.84
Entire area		4.2	8.6	2.65	1.83	3.45	0.79	3.35	0.72

The diagrams related to seismicity parameters estimation by applying the maximum-likelihood method proposed by Kijko and Sellevoll (1992) and Kijko (2004) are shown in Fig. 11.
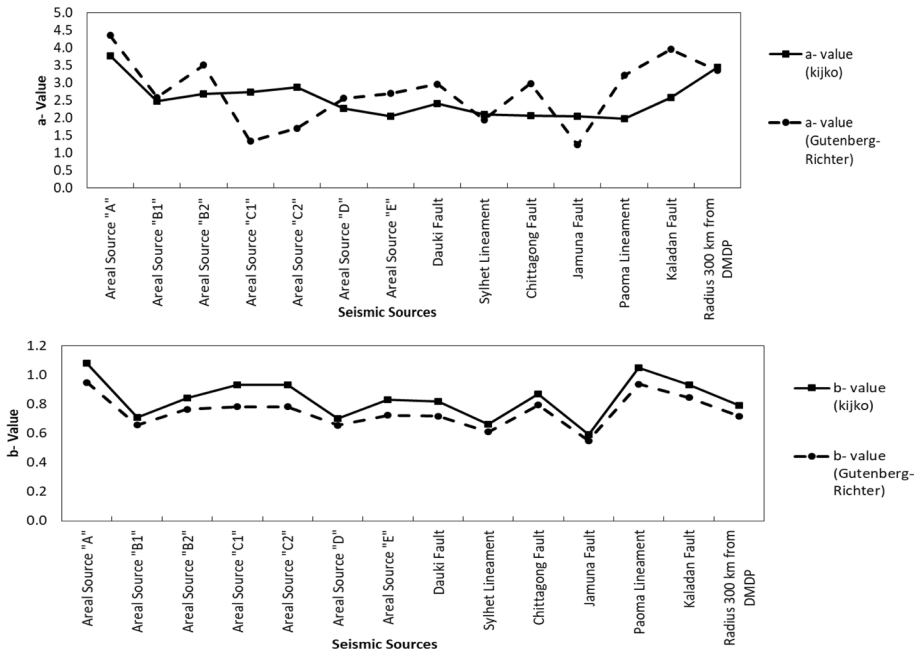
Fig. 10 Variation of a- and b-value estimation

2.6 Maximum magnitude estimation

The M_{max} values for linear sources are calculated with relationships proposed by Wells and Coppersmith (1994), Blaser et al. (2010), Strasser et al. (2010), Mohajer-Ashjai and Nowroozi (1978), and Ambraseys and Jackson (1998). M_{max} then has been averaged between values calculated by mentioned relationships, estimated M_{max} calculated by Kijko (2004), M_{max} obtained in double-truncated Gutenberg–Richter model, and maximum observed assigned earthquake to each fault (Table 5). For areal sources, the M_{max} values have been averaged between the estimated M_{max} calculated by Kijko (2004) and the maximum assigned earthquake to each source (Table 6).

To calculate the Z_{TOR}, the method suggested by Kaklamanos et al. (2011) is used. Some GMPEs require two site parameters termed $Z_{1.0}$ (a depth where $V_S = 1$ km/s) and $Z_{2.5}$ (a depth where $Vs = 2.5$ km/s). Here, the relationship proposed by Chiou and

Table 5 M_{max} assigned to each linear seismic source

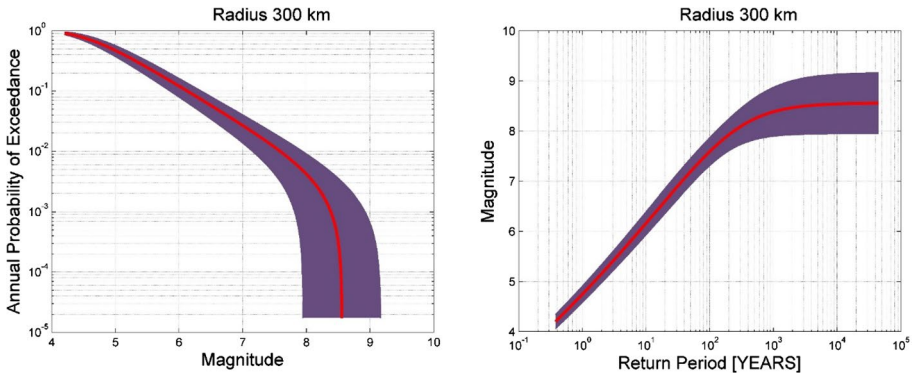| Name	Final Mw	Std	Name	Final Mw	Std
CCF1	7.2	0.52	DaF_W	7.4	0.43
CCF2	6.8	0.54	JF	6.5	0.40
CCF3	7.2	0.52	MaF	6.9	0.42
CCF4	7.1	0.50	KaF1	7.1	0.40
DaF_E	7.1	0.41	KaF2	7.3	0.42
DaF_Em	6.6	0.53	KaF3	7.5	0.48
DaF_C	7.6	0.39	PaL1	6.6	0.38

Fig. 11 Diagrams resulted from the calculation of seismicity parameters

Youngs (2014) has been applied to estimate $Z_{1.0}$. To estimate $Z_{2.5}$, Campbell and Bozorgnia (2007) proposed a method, which is used here.

2.7 Focal depth

A three-dimensional seismicity model has been prepared along with topography and faults to study and determine the depth of the seismogenic layer. The distribution of earthquake depths for the developed instrumental catalog in the present study is shown in Fig. 12a. Most earthquake depths are 9–15 km and 33–37 km. Therefore, two statistical models can be seen in the histogram of earthquake depths. As regards, depths reported in routine bulletin locations are fixed at an arbitrary depth (33 km for the USGS and ISC) (Jackson 2001), the earthquake depths in the range of 33–37 km have been removed, and only one mode appears with an average value of 10 km. Figure 12b shows the seismogenic layer depth between 9 and 15 km (with a bold symbol) with an even distribution throughout the 300-km radius of DMR.

On the other hand, the catalog of ISC-EHB Bulletin (events from 1964 to 2016) minimizes errors in locations and particularly depth by applying procedures described by Engdahl et al. (1998), which has been used for earthquake depth investigation in the present study. The ISC-EHB catalog is depicted as a three-dimensional model, and the seismogenic

Table 6 M_{max} assigned to each seismic areal source

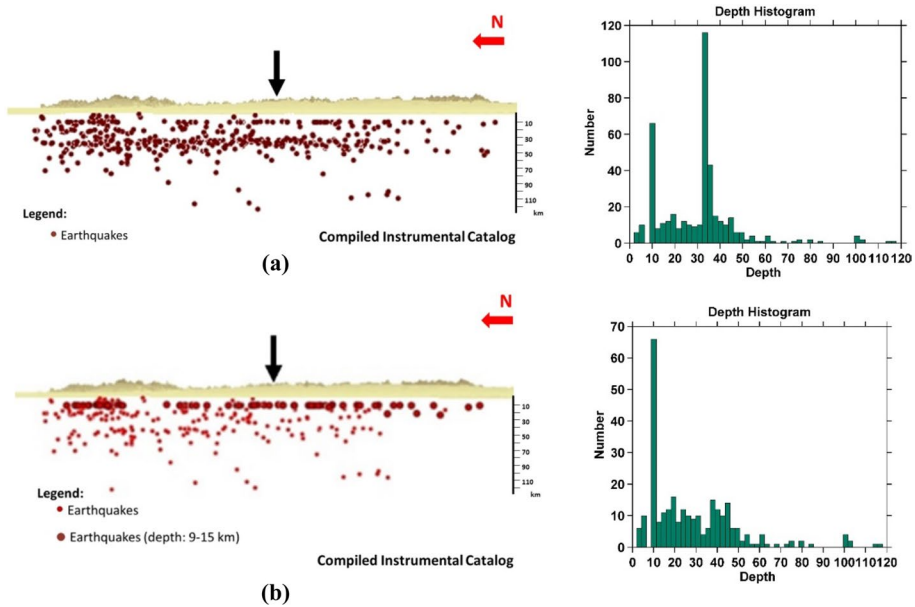| Name	Kijko (2004)			Gutenberg–Richter model	Observed M	Final Mw	Std
	M	M -δ	M + δ	M			
A	6.3	6.0	6.6	6.6	6.1	6.3	0.27
B1	6.0	5.7	6.4	6.9	6.3	6.3	0.44
B2	6.3	6.0	6.6	8.1	6.3	6.7	0.80
C1	6.4	6.1	6.7	6.4	6.3	6.4	0.22
C2	6.4	6.1	6.7	6.4	6.3	6.4	0.22
D	6.0	5.6	6.3	6.7	5.8	6.1	0.39
E	6.4	5.7	7.1	5.9	6.8	6.4	0.52

Fig. 12 Two-dimensional model of earthquake depth based on compiled instrumental catalog

layer is obtained from 10 to 15 km (Fig. 13). In addition, according to Spence (1989), the earthquake depth range of 0–700 km can be divided into shallow, intermediate, and deep. Shallow earthquakes are between 0 and 70 km, intermediate earthquakes have 70–300-km depth, and deep earthquakes have 300–700-km depth. Based on this classification, the majority of occurred events are shallow earthquakes. The depth of the seismogenic layer has been considered between 9 and 15 km for the present study.
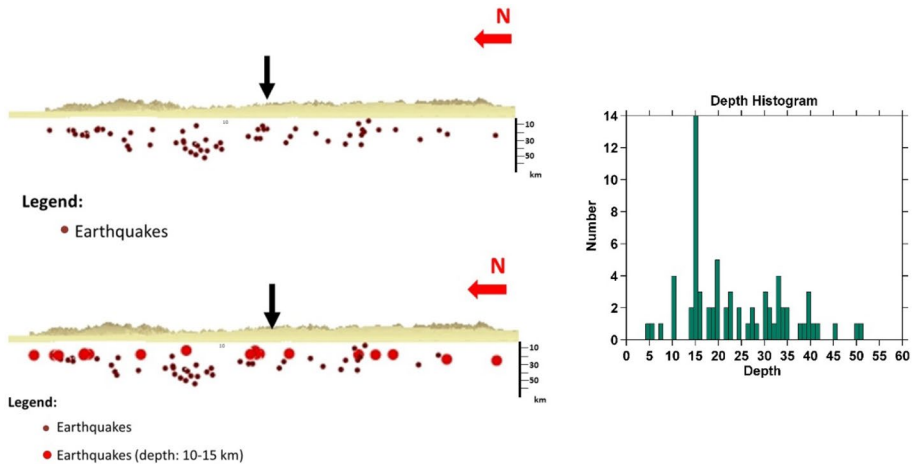

Fig. 13 Two-dimensional model of earthquake depth based on ISC-EHB catalog

Table 7 List of earthquakes used for GMPEs ranking

Earthquake	Date and Time (UTC)	Lat	Lon	Depth (km)	Mw	Ms	M (other)	No. of Records
Bhuj—Kachchh	2001–01-26 03:16:40	23.42	70.23	16	7.7			1
Chamoli	1999–03-28 19:05:11	30.51	79.40	15	6.6			11
India–Burma Border 1997	1997–05-08 02:53:15	24.89	92.25	34	6.0	5.6		11
India–Burma Border 1995	1995–05-06 01:59:07	24.98	95.29	117	6.4			9
Uttarkashi	1991–10-19 21:23:15	30.78	78.77	10		7		13
India–Burma Border 1990	1990–01-09 18:51:29	24.75	92.24	119			6.1	14
India–Burma Border 1988	1988–08-06 00:36:25	25.14	95.12	90	7.3	7.2		33
India–Bangladesh Border	1988–02-06 14:50:45	24.68	91.57	15	5.9	5.8		18
India–Burma Border 1987	1987–05-18 01:53:51	25.27	94.20	49	6.3	5.9		14

2.8 GMPE selection

Selecting appropriate GMPEs capable of estimating proper ground motion parameters is one of the challenges in any SHA. This is particularly apparent in regions where local GMPEs do not exist. The main common approaches to distinguish between different models and critic their validity are the likelihood (LH), log-likelihood (LLH), and Euclidean distance-based ranking (EDR). For GMPEs ranking, the dataset of records relative to earthquakes in India has been collected. The dataset is composed of 124 records related to nine events (Table 7). A literature review has been carried out to identify potential candidate GMPEs within the study area considering the tectonic environment. Table 8 gives the name of GMPEs that are used by different researchers for similar regions and applied as input for the ranking process in this paper.

The spectral acceleration was generated using the candidate GMPEs over six periods (0.0 s, 0.1 s, 0.2 s, 0.5 s, 1.0 s, and 2 s) for all ground motion records in the selected dataset. Then, their fitness to the dataset is analyzed by applying LH, LLH, and EDR approaches (Figs. 14 and 15). As a result, the GMPEs proposed by Abrahamson and Silva (1997), Sharma et al. (2009), Boore et al. (1997), and Campbell and Bozorgnia (2008) are selected for the active shallow crustal regime. Also, the relations by Toro (2002) Tavakoli and Pezeshk (2005), Atkinson and Boore (2006), and Campbell (2003) are nominated for the stable shallow crustal regime.

Table 8 List of GMPEs used as input for the ranking process

| GMPE	Tectonic region	The papers that used the mentioned GMPE
Zhao et al. 2016	Active shallow crust	(Haque et al. 2019)
Chiou and Youngs 2014	Active shallow crust	(Haque et al. 2019)
Nath et al. 2012	Subduction interface	(Haque et al. 2019)
Atkinson and Boore 2011	Stable shallow crust	(Haque et al. 2019)
Pezeshk et al. 2011	Stable shallow crust	(Ashish et al. 2016)
Akkar and Bommer 2010	Active shallow crust	(Haque et al. 2019; Ashish et al. 2016a; Kolathayar et al. 2012; Nath and Thingbaijam 2012)
Sharma et al. 2009	Active shallow crust	(Kolathayar et al. 2012; Nath and Thingbaijam 2012)
Chiou and Youngs 2008	Active shallow crust	(Ashish et al. 2016b; Bendimerad and Morrow 2014; Nath and Thingbaijam 2012)
Boore and Atkinson 2008	Active shallow crust	(Bendimerad and Morrow 2014; Kolathayar et al. 2012; Nath and Thingbaijam 2012)
Campbell and Bozorgnia 2008	Active shallow crust	(Haque et al. 2019; Bendimerad and Morrow 2014)
Abrahamson and Silva 2008	Active shallow crust	(Haque et al. 2019; Bendimerad and Morrow 2014)
Lin and Lee 2008	Subduction interface	(Haque et al. 2019)
Raghu Kanth and Iyengar 2007	Stable shallow crust	(Kolathayar et al. 2012; Nath and Thingbaijam 2012)
Zhao et al. 2006	Active shallow crust	(Bendimerad and Morrow 2014; Nath and Thingbaijam 2012)
Atkinson and Boore 2006	Stable shallow crust	(Haque et al. 2019; Ashish et al. 2016b; Kolathayar et al. 2012; Nath and Thingbaijam 2012)
Tavakoli and Pezeshk 2005	Stable shallow crust	(Haque et al. 2019; Nath and Thingbaijam 2012)
Campbell and Bozorgnia 2003	Active shallow crust	(Kolathayar et al. 2012)
Atkinson and Boore 2003	Subduction interface	(Haque et al. 2019)
Campbell 2003	Stable shallow crust	(Nath and Thingbaijam 2012)
Toro 2002	Stable shallow crust	(Nath and Thingbaijam 2012)
Abrahamson and Silva 1997	Active shallow crust	(Al-Hussaini et al. 2015; Al-Hussaini and Al-Noman 2010)
Boore et al. 1997a	Active shallow crust	(Sarker et al. 2010)
Youngs et al. 1997	Subduction interface	(Haque et al. 2019; Bendimerad and Morrow 2014)
Atkinson and Boore 1995	Stable shallow crust	(Al-Hussaini and Al-Noman 2010)
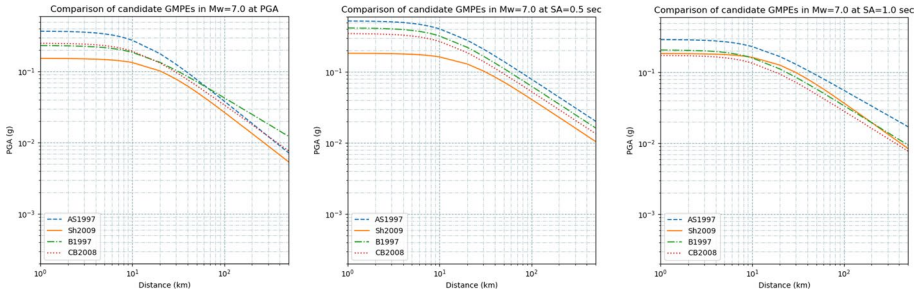
Fig. 14 Comparison of selected active shallow crustal GMPEs in periods of 0 s, 0.5 s, and 1 s for Mw = 7.0
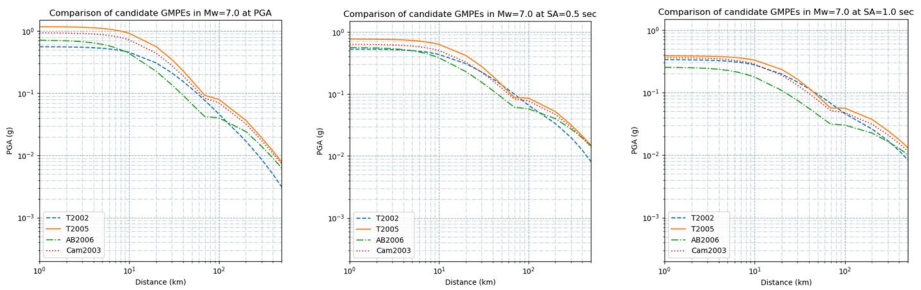

Fig. 15 Comparison of selected stable shallow crustal GMPEs in periods of 0 s, 0.5 s, and 1 s for Mw = 7.0

2.9 Logic tree analysis

The logic tree contains different weights for source models, magnitude–frequency distribution models, maximum magnitudes, depths, nodal planes, and GMPEs. Figure 16 shows the defined logic tree which is used in this study.

2.10 Classical PSHA on bedrock

The calculation is done using the OpenQuake engine. Figure 17 shows the PGA map for return periods of 475 and 2475 years on bedrock. Seismic bedrock is considered where the V_{S30} reaches the value between 760 and 800 m/s, according to BNBC (Ministry of Housing & Public Works 2020). The PGA values calculated by classical PSHA change between 0.14–0.19 and 0.33–0.46 on bedrock for a return period of 475 and 2475 years, respectively.

2.11 Scenario-based SHA on bedrock

In this method, the controlling earthquake is assumed to act along with the source at the closest distance from the site. The scenario-based SHA has been carried out for various scenarios including, CCF segment 1, CCF segment 2, Dauki Fault (central segment), Dauki Fault (eastern segment), Dauki Fault (easternmost segment), Dauki Fault (western segment), Jamuna Fault, Jamuna Fault (Madhupur segment), Kaladan Fault 1, Kaladan
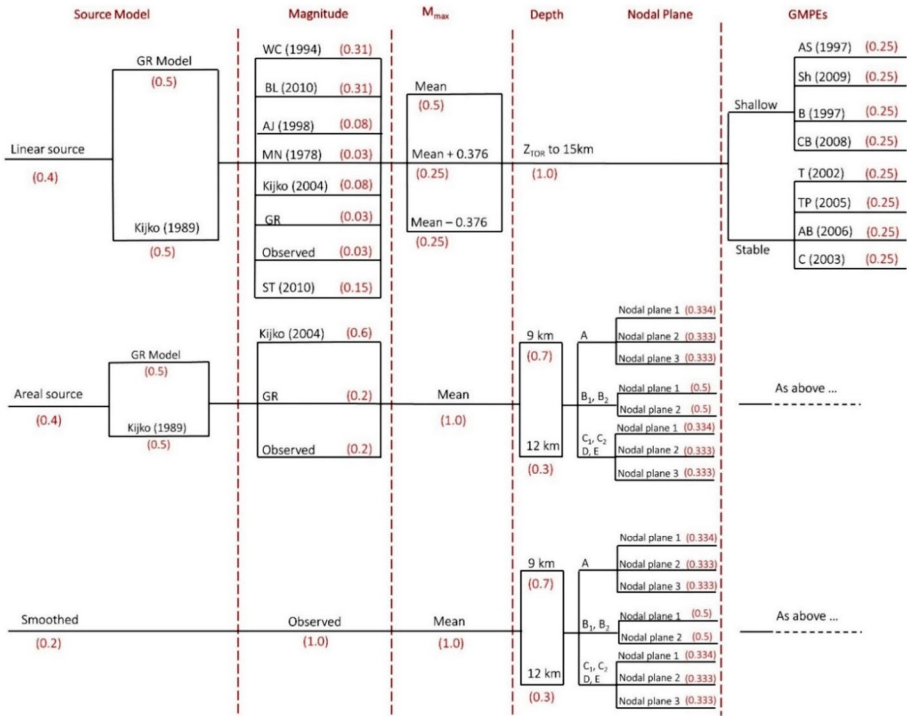
Fig. 16 The logic trees

Fault 2, Paoma lineament 2, Paoma lineament 3, and Sylhet lineament. The PGA maps of the worst-case scenario (Madhupur and Sylhet Faults) are shown in Fig. 18.

3 Seismic site response analysis in DMR

The previous earthquakes show that the seismic damages are controlled by five main components, namely, seismic sources, path characteristics, local soil, geotechnical characteristics, and, finally, the structural design of buildings (Sitharam et al. 2018). In the previous sections, the effect of seismic source and path characteristics have been evaluated in the assessment of ground motion on bedrock. The seismic site response analysis is conducted by assessing the effects of soil conditions. Thus, the surface motion and site amplification factors are calculated by defining the sub-surface soil type and the variation of their properties with depth.

3.1 Site characterization

Here, the input data come from more than 14,000 m of SPT boreholes at 378 locations and more than 15,000 m of SDHT at 400 locations. In addition, 400 drilled boreholes have been considered for lithological modeling and interpretation. Soil modeling was performed using interpolated data in the desired range by applying the anisotropic inverse distance
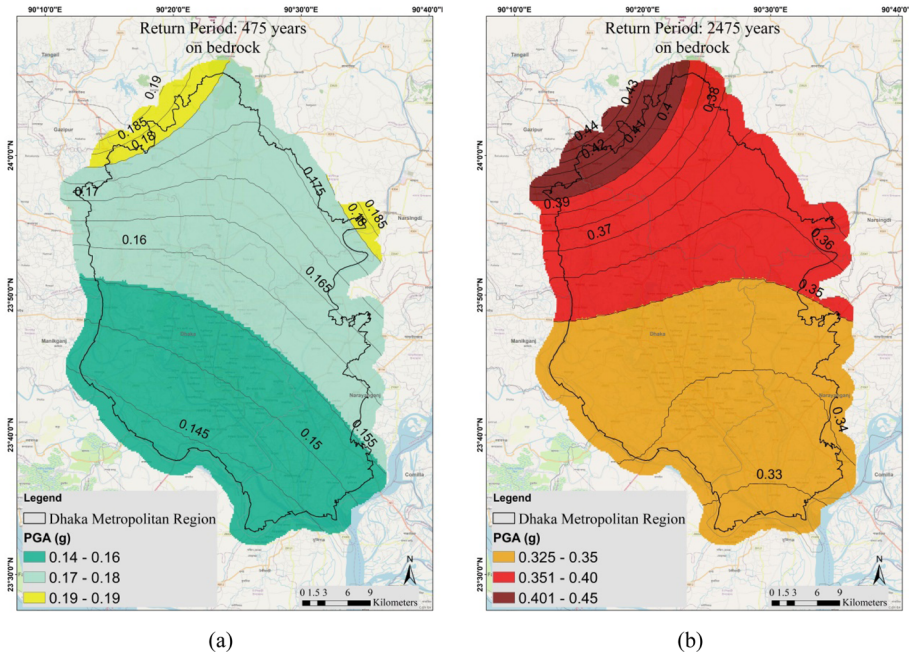
Fig. 17 The PGA map for bedrock for different return periods; **a** 475 years and **b** 2475 years
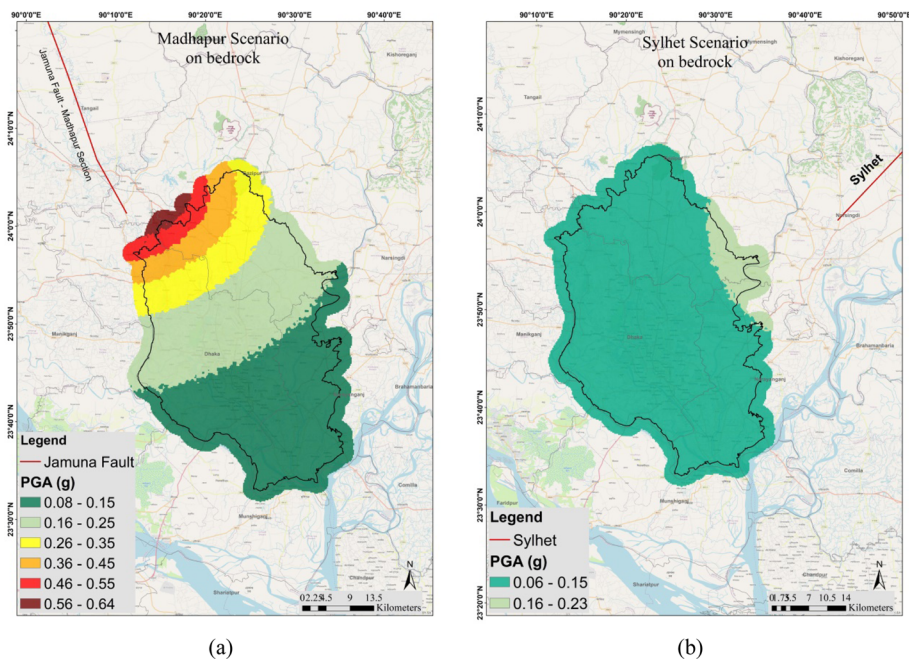

Fig. 18 The scenario-based PGA map on the bedrock for **a** Madhupur and **b** Sylhet Faults
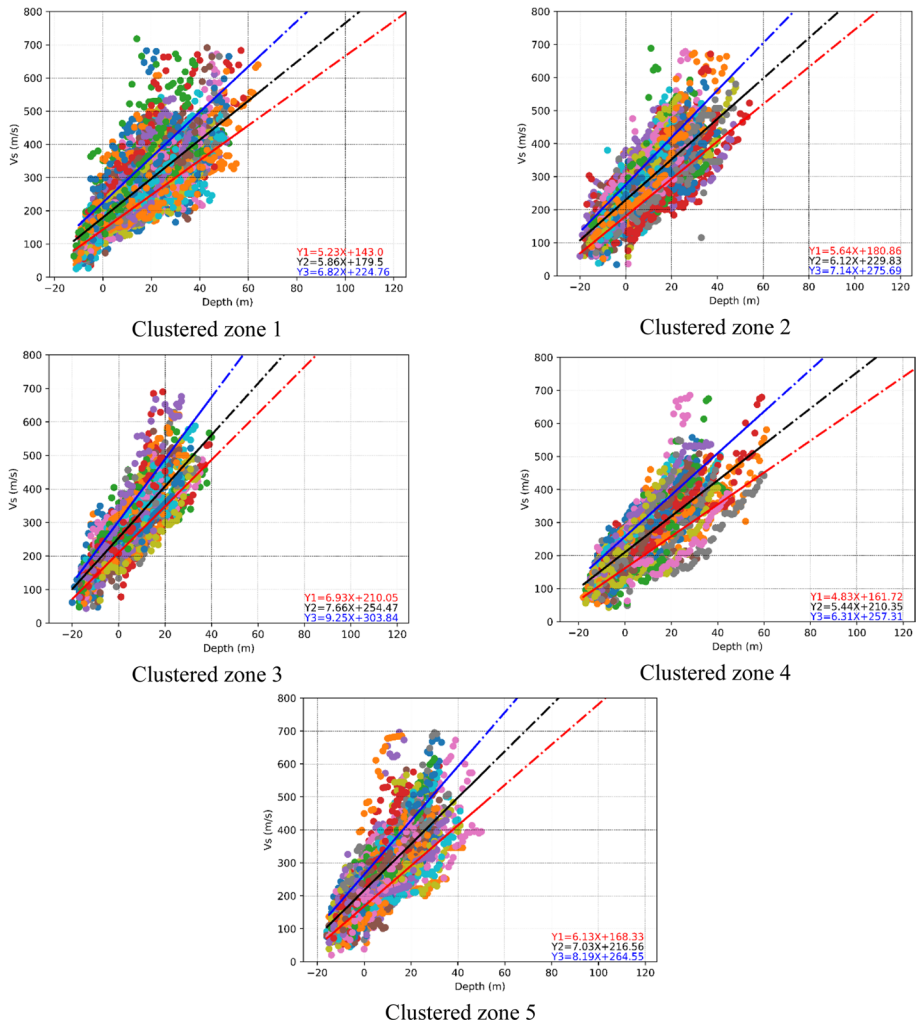
Fig. 19 The assigned relationship to find the depth of seismic bedrock for various clustered zones

weighting (IDW) method at the other points. Based on the V_{S30} values, the soil type based on BNBC-2020 in DMR is classified as "SC" and "SD."

A clustering map has been prepared to apply the SOM (Self-Organizing Map) method to select a certain number of SDHT out of the total drilled boreholes. For this purpose, six layers containing amplification, natural frequency, V_{S30}, long-term bearing capacity, short-term bearing capacity, and the average of SPT have been considered as the input layer, and finally, five zones have been determined as the optimum number of clusters in the DMR. Considering the area of each cluster and designing a regular fishnet, 58 boreholes located as near as possible to the center of each cell have been selected for further analysis related to the site effect.

Table 9 Selected ground motion on the seismic bedrock

Earthquake		Station									Max Acc. (g)	
Eq. name	Date and time (UTC)	M type	M	depth (km)	Station name	Abb	Lat	Lon	Hypo. Dist. (km)	V_{S30} (m/s)	Component H1	Component H2
India–Burma Border	1987–05-18 01:53:51	Mw	6.3	49	Hatikhali	B87_Ha	25.93	93.07	127.1	900	0.037	0.030
					Laisong	B87_La	25.12	93.19	102.3	900	0.060	0.042
India–Burma Border	1988–08-06 00:36:25	Mw	7.3	90	Dauki	B88_Da	25.12	92.02	324.7	846	0.106	0.070
India–Burma Border	1990–01-09 18:51:29	Other	6.1	119	Laisong	B90_La	25.12	93.19	233.5	900	0.055	0.061
India–Burma Border	1995–05-06 01:59:07	Mw	6.4	117	Hatikhali	B95_Ha	25.93	93.07	262.6	900	0.042	0.044
Chamoli	1999–03-28 19:05:11	Mw	6.6	15	Almora	C99_Al	29.35	79.39	96.1	900	0.026	0.027
					Barkot	C99_Ba	30.48	78.13	123.7	900	0.022	0.017
					Chinaylisaur	C99_Ch	30.33	78.2	106.7	900	0.044	0.051
					Ghansiali	C99_Gh	30.25	78.39	75.3	870	0.082	0.071
					Joshimath	C99_Jo	30.33	79.34	26	900	0.070	0.062
NE India	1986–09-10 07:50:26	Ms	4.5	43	Dauki	I86_Da	25.12	92.02	50.9	846	0.089	0.090
India–Bangladesh Border 1988–02-06	1988–02-06 14:50:45	Mw	5.9	15	Dauki	I88_Da	25.12	92.02	80.5	846	0.026	0.038
					Hatikhali	I88_Ha	25.93	93.07	195.5	900	0.025	0.023
Uttarkashi	1991–10-19 21:23:15	Ms	7	10	Almora	U91_Al	29.35	79.39	153.5	900	0.017	0.021
					Barkot	U91_Ba	30.48	78.13	55.8	900	0.081	0.093
					Bhatwari	U91_Bh	30.48	78.36	21.7	900	0.248	0.242
					Ghansiali	U91_Gh	30.25	78.39	39.3	870	0.115	0.116
					Koteshwar	U91_Kt	30.14	78.34	61.3	831	0.065	0.099
					Koti	U91_Ko	30.35	77.47	98.7	900	0.041	0.021
					Purola	U91_Pu	30.52	78.05	70	847	0.074	0.092

3.2 Seismic bedrock position

Ground motion prediction equations are more reliable to estimate ground motion parameters for bedrock. Since the boreholes are not reached the bedrock and the shear wave velocity of 800 m/s (as seismic bedrock), seismic bedrock should be defined using the extrapolation approach. For this purpose, the shear wave velocity for each depth obtained in SDHTs was used to develop the extrapolation method. Figure 19 shows the assigned relationships for each clustered zone. In each diagram, three lines and their formula have been shown obtained by applying linear regression. The black line was taken as the average value of the shear wave velocity at each depth. Also, the blue and red lines are relevant to the upper and lower band of average regression, respectively.

3.3 Input ground motion selection

In general, for a seismic site response analysis, it is essential to select proper ground motion records under similar seismic conditions of the study site. Similar seismic conditions contain earthquake magnitude, fault mechanism, local soil condition, and the site's distance to the seismic source (Iervolino and Cornell 2005; Jia and Jia 2018). The selected ground motion records for the current study are shown in Table 9.

The selected records should be modified to be consistent with a specific target response spectrum. The seismic spectrum can be defined in different approaches, namely, deterministic, PSHA, and building codes (Rathje et al. 2010). The design spectra provided in BNBC 2020 for rock (site class: SA) have been used as the target spectrum in the current study. Scaling and spectral matching are two methods used for modifying the time series to be consistent with the target spectrum (al Atik and Abrahamson 2010). By applying the modifying procedures, the records will be matched within the specified period range, and the scatter in the response spectra will be decreased after scaling (Ansal et al. 2018). In the present study, spectral matching which involves modifying the frequency content of the earthquake records to match the defined target spectrum at all spectral periods has been adopted. Figure 20 and Fig. 21 show the comparison between the original and matched time history and spectrum for the U91Bh record.

3.4 Seismic hazard on the surface

The effect of site characteristics on the ground motion, site amplification, and the concentration of earthquake damages in various regions are found to be relevant to the local soil conditions (Phillips and Aki 1986; Stewart et al. 2003; Pitilakis 2004). The dynamic simulation propagates earthquake time histories through the soil profile to assess surface acceleration and amplification factors. Several numerical approaches have been used for one-dimensional seismic site response analysis, including the time-domain nonlinear (NL) method (Qodri et al. 2021) and the frequency-domain equivalent-linear (EQL) method. In the current study, the amplification factor and the surface motion parameter have been estimated using the frequency-domain equivalent-linear approach. It should be mentioned that to investigate the validity of applying the equivalent-linear approach, the maximum strain of each layer in the soil profile has been checked, and it was in the acceptable range.
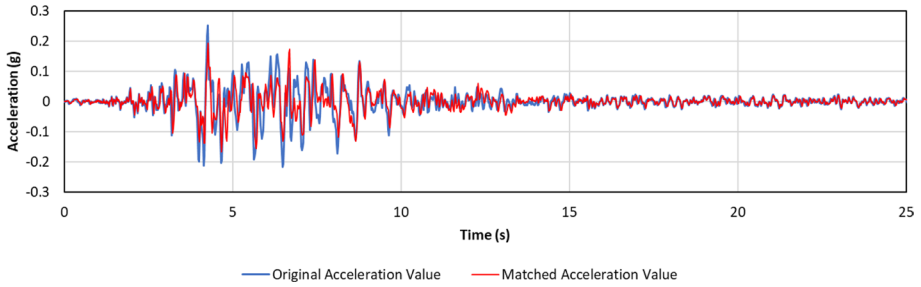
Fig. 20 The comparison between the original and matched time history for the "U91Bh" record
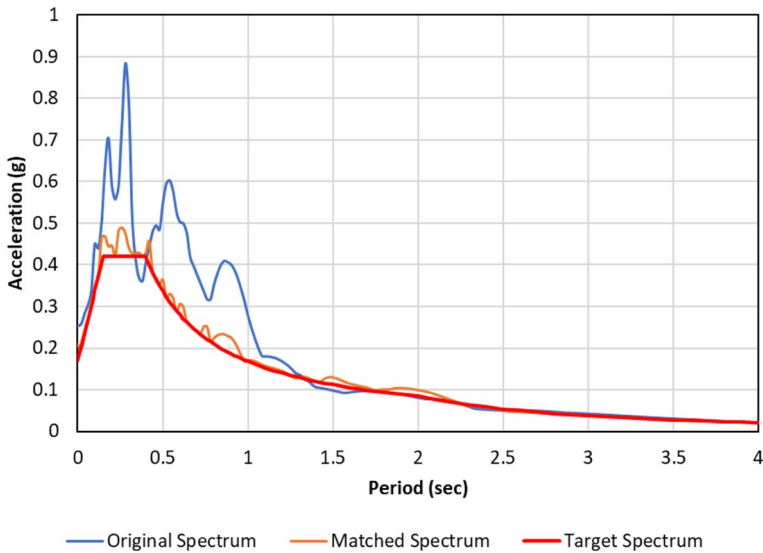

Fig. 21 The comparison between the original, matched, and target spectrum for the "U91Bh" record

The main required parameters for the equivalent-linear approach are the shear wave velocity, unit weight, and thickness of each layer in the soil profile. Other factors to estimate ground response analysis are the modulus reduction and damping versus strain curves. The selected empirical curve based on the local expert advice in Bangladesh is Seed and Idriss (1970) and Vucetic and Dobry (1991) for sand and clay, respectively. The calculated amplification factor is shown in Fig. 22. The PGA zonation map on the surface for both probabilistic (return periods of 200, 475, and 2475 years) and scenario-based (Madhupur and Sylhet Faults) approaches is presented in Fig. 23 and Fig. 24, respectively.

3.5 Response spectrum determination in DMR

A response spectrum curve is used to show the earthquake loading. It is a spectrum of peak responses in terms of acceleration, velocity, or displacement of a group of single-degree-of-freedom (Jia 2016). In the present study, to provide a surface response spectrum, DMR was classified into three classes based on the changes in surface acceleration. The variation of surface PGA in classes 1, 2, and 3 is less than 0.25 g, between 0.25 g and 0.3 g, and greater than 0.3 g, respectively. Also, according to the BNBC 2020, the seismic zone coefficient (Z) that represents the maximum PGA for site class SA is 0.2 (Zone 2) for most of DMR, except for the northern part of DMR where the zone coefficient is 0.28 (Zone 3). Since some parts of the third class are located in areas with a zone coefficient is 0.28, it has been classified into two groups based on the variation of the seismic zone coefficient.

The soil dynamic analysis has been carried out by propagating rock acceleration time histories (selected input motion presented in Table 9) through the local soil profiles located in each class. The results of surface response spectra in the four mentioned classes containing the response spectrum of each input motion, average spectrum, and average ± one standard deviation are provided in Fig. 25.

3.6 Design spectra

The seismic design philosophy of ASCE 7–16 defines the design earthquake as "the earthquake effects that are two-thirds of the corresponding Maximum Considered Earthquake
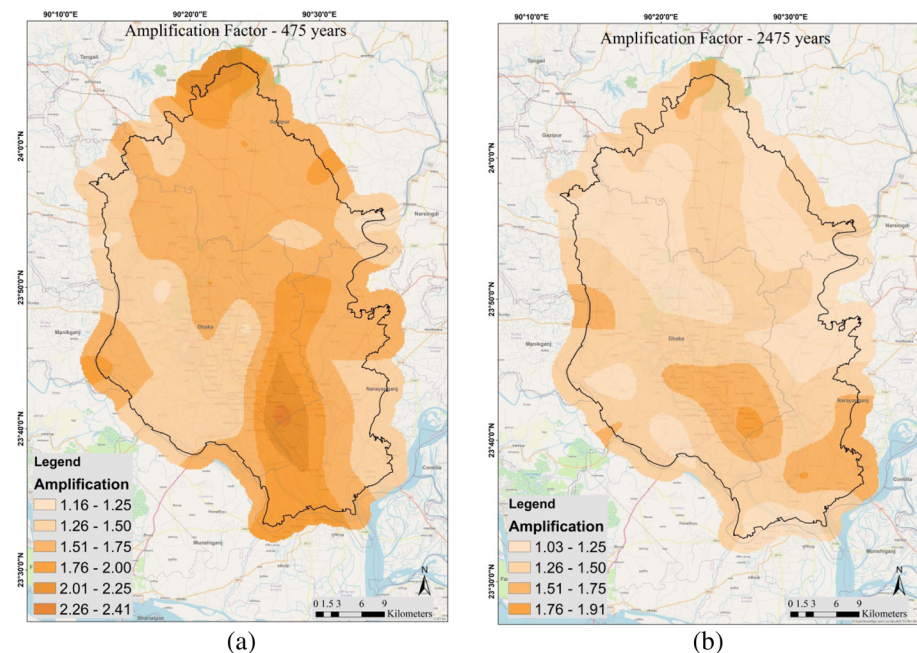

Fig. 22 Amplification factors for various return periods; **a** 475 years and **b** 2475 years
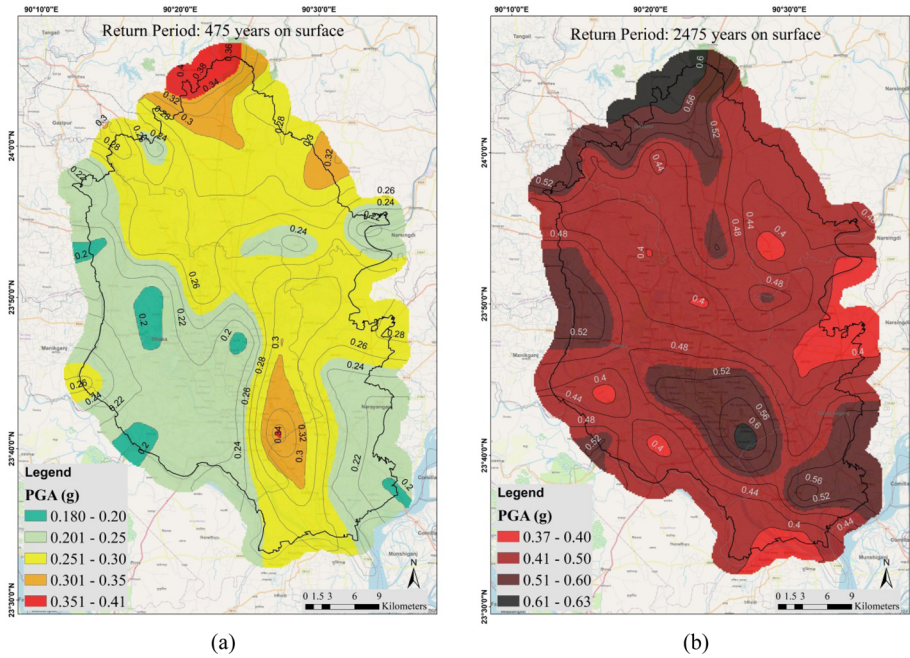
Fig. 23 PGA on the surface for various return periods using classical PSHA; **a** 475 years and **b** 2475 years
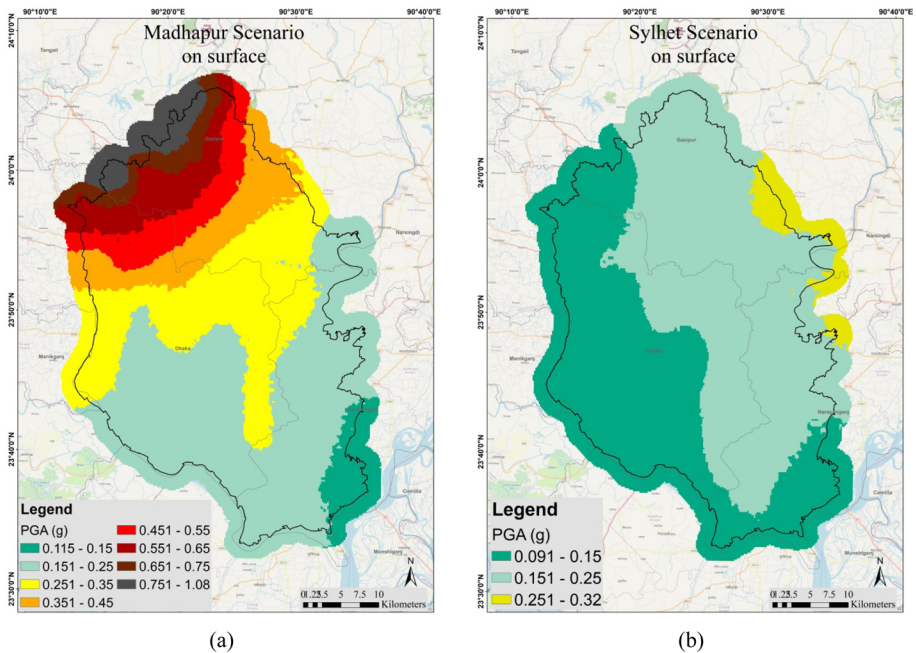

Fig. 24 Scenario-based PGA map on the surface for **a** Madhupur Fault and **b** Sylhet Fault

effects" (ASCE 2017). Also, based on this standard, the site-specific spectrum at any period shall not be taken as less than 80% of the standard design spectra. The final design spectra in four classes have been proposed and compared with the ASCE 7–16 spectrum (calculated for site class D) (Fig. 26).

4 Discussion and Conclusions

The classical PSHA and scenario-based SHA have been calculated over DMR in 10,000 sites (about 500 * 500 m). Applying the seismic site response analysis and the seismic downhole test data, the effect of soil condition is evaluated; and site amplification factors and the surface motion are calculated. Table 10 presents the range of estimated PGA on bedrock and surface for DMR.

Comparing the results of this paper with the literature does not show a meaningful contradiction. Although, the procedure has been improved in this paper, and a comprehensive set of results are exhibited (zonation maps and bedrock and surface, response spectrum, design spectrum, amplification factor, and the soil model). To cite an instance, Kolathayar et al. (2012) have completed a deterministic SHA in India, which also includes the study area of this study. Their results show a PGA from 0.1 g to 0.25 g
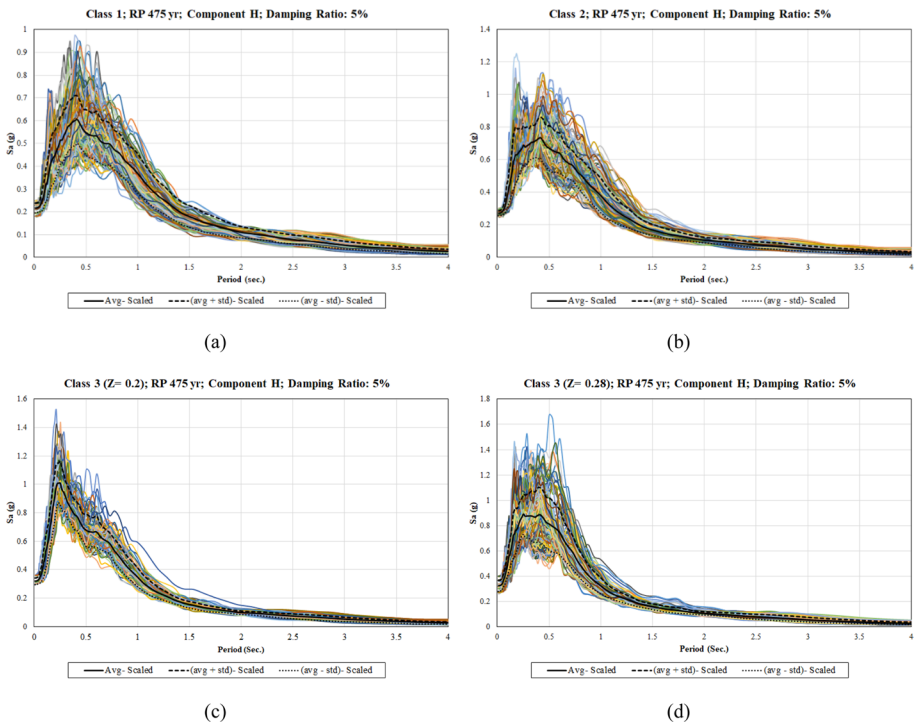

Fig. 25 The scaled surface response spectrum (horizontal component) for the return period of 475 years and a damping ratio of 5% in **a** class 1, **b** class 2, and **c** class 3 with a zone coefficient of 0.2, and class 3 with a zone coefficient of 0.28 (the colored curves are the response spectra obtained based on various input motions and soil profiles)

for Dhaka on a bedrock level. In their logic tree, two source models (linear and point) and three GMPEs for each tectonic condition are considered, and other parameters, such as magnitude or depth, are not included. Also, all the results are presented for bedrock, and the soil condition is not considered. Nath and Thingbaijam (2012) did a remarkable probabilistic SHA in India. They used the logic tree approach and a GMPE ranking to reduce the uncertainty of results. But the results of this study also express just the level of seismic hazard on bedrock, and no site effect analysis has been completed. The most recent studies in the target area are accomplished by Haque et al. (2019) and Rahman et al. (2020). The study of Haque et al. (2019) is the only recently published paper that considered the site effect and calculated the PGA for the surface. However, the vs30 model used in this study is built from 178 boreholes data for entire Bangladesh. Of these 178, only eight data points were located in the DMR, which put the uncertainty of the model at a very high level. Rahman et al. (2020) have accounted for the epistemic uncertainties using the logic tree approach. They defined four source types and disaggregate the results to show the most probable scenario. Yet, this paper also calculated the hazard level just on the engineering bedrock. To sum up the comparison of the results with the previous works, the following points should be noted.

First, the current research is focused on the great Dhaka area. Since Dhaka is the most populated city and the capital of Bangladesh, the occurrence of an earthquake not only put approximately 20 million inhabitants at risk but also the crisis management
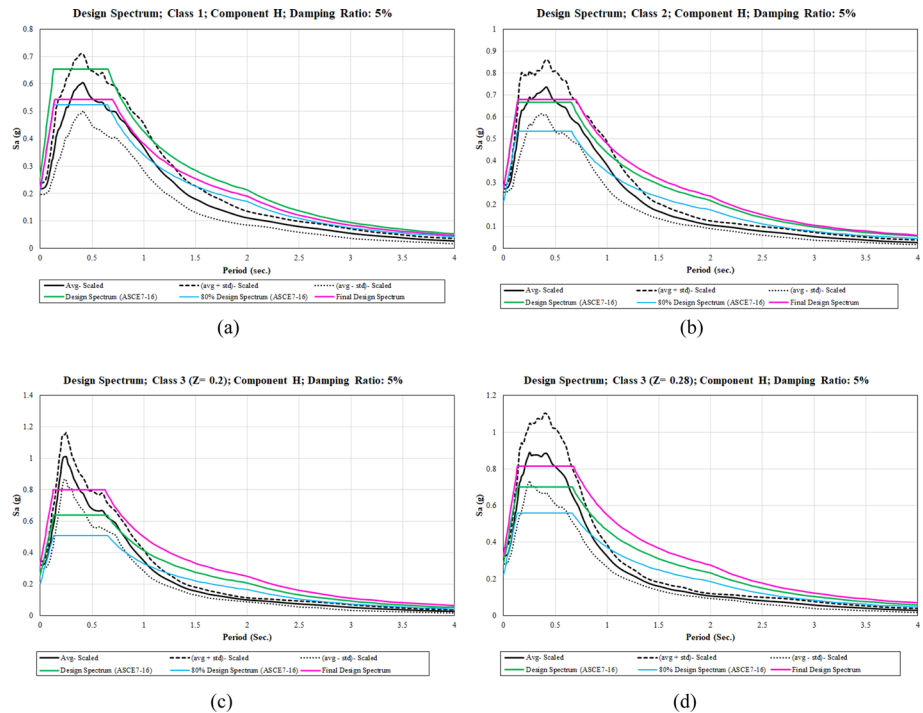

Fig. 26 Final design spectra (horizontal component) for a damping ratio of 5% in BH4 in comparison with ASCE 7–16 in **a** class 1, **b** class 2, **c** class 3 with a zone coefficient of 0.2, and **d** class 3 with a zone coefficient of 0.28

Table 10 Summary of DMR seismic hazard analysis

Seismic hazard level/case	Scenario magnitude	PGA (g) bedrock	PGA (g) surface	
Probabilistic	50 years		0.03–0.05	0.05–0.10
	75 years		0.04–0.07	0.07–0.14
	100 years		0.06–0.08	0.09–0.18
	200 years		0.09–0.13	0.14–0.29
	475 years		0.14–0.19	0.18–0.41
	2475 years		0.33–0.46	0.37–0.63
	10,000 years		0.61–0.80	0.67–1.21
Scenario-based	CCF (segment 1)	7.2	0.06–0.10	0.07–0.19
	CCF (segment 2)	6.8	0.04–0.06	0.05–0.18
	Dauki (central segment)	7.6	0.04–0.07	0.06–0.14
	Dauki (eastern segment)	7.1	0.03–0.04	0.04–0.08
	Dauki (easternmost segment)	6.6	0.02–0.025	0.03–0.05
	Dauki (western segment)	7.4	0.04–0.065	0.06–0.13
	Jamuna	6.5	0.04–0.08	0.05–0.18
	Jamuna (Madhapur segment)	6.9	0.08–0.68	0.12–0.9
	Kaladan (segment 1)	7.1	0.03–0.04	0.03–0.07
	Kaladan (segment 2)	7.3	0.03–0.04	0.04–0.08
	Paoma (segment 2)	6.9	0.03–0.04	0.03–0.08
	Paoma (segment 3)	7.0	0.05–0.11	0.06–0.19
	Sylhet	7.1	0.07–0.24	0.09–0.32

would be very brittle as the capital is involved. Therefore, although there have been studies for Bangladesh, a detailed investigation of Dhaka and its development area was indispensable.

The second point is that in this paper, one aim was to reduce the uncertainties. In this regard, the calculation is carried out in 10,000 points to decrease the effect of interpolation as much as possible. Also, in logic three, every probable state for source models, magnitude, seismicity parameters, focal depth, nodal planes, and GMPEs are included. The logic tree presented in this paper is the most complicated one used for the region.

The third exclusivity is that to select the proper GMPE, unlike most of the previous research, the ranking procedure has been done. Initially, 24 relations have been nominated by reviewing papers in similar regions. Then, EDR, LH, and LLH algorithms were applied, and in conclusion, eight GMPEs (four active shallow crust and four stable shallow crust) have been chosen. Subsequently, it can be said that the applied relations are the most compatible ones.

The fourth and most advantage of this research compared to earlier works is to model the soil profile with a one-dimensional frequency-domain equivalent-linear analysis, express the amplification factor, and represent the PGA and design spectra on the surface. This modeling has been completed using a dense dataset from 400 SDHT and 378 SPT which makes the model completely reliable.

In Table 11, the results from other studies are compared. It can be seen that the PGA calculated for the surface in this study goes up to 0.41 g which shows a higher level of hazard for the region. Regarding the soil condition of the area, it is recommended to consider

Table 11 The comparison of the classical PSHA on bedrock for a return period of 475 years with various previous studies

Study name	Author	Location of study	PSHA	DSHA	GMPE ranking	Logic tree	Site effect	PGA (g)
Seismic source modeling and probabilistic seismic hazard analysis for Bangladesh	(Rahman et al. 2020)	Bangladesh	Yes	No	No	Yes	No	0.1–0.2 [a]
Toward improved probabilistic seismic hazard assessment for Bangladesh	(Haque et al. 2019)	Bangladesh	Yes	No	No	Yes	Used 178 data for the entire Bangladesh (8 data for DMR)	0.18–0.34 [b]
Probabilistic seismic hazard assessment of India	(Nath and Thingbaijam 2012)	India	Yes	Yes	Yes	Yes	No	0.2–0.28 [a]
Deterministic seismic hazard macro-zonation of India	(Kolathayar et al. 2012)	India	No	Yes	No	Yes	No	0.1–0.25 [a]
Probabilistic estimates of PGA and spectral acceleration in Bangladesh	(Al-Hussaini and Al-Noman 2010)	Bangladesh	Yes / Yes	No / No	No / No	No / No	No / No	0.093–0.156 [a,c] / 0.095–0.193 [a,d]
Global seismic hazard assessment program	(Zhang et al. 1999)	Continental Asia	Yes	No	No	No	No	0.08–0.24 [a]
A probabilistic seismic hazard map of India and adjoining regions	(Bhatia et al. 1999)	India	Yes	No	No	No	No	0.20–0.25 [a]
Seismic hazard assessment of Dhaka, Chittagong, and Sylhet Corporation area of Bangladesh	Comprehensive Disaster Management Program (CDMP) (2009)	Dhaka	Yes	Yes	No	No	Yes	0.1–0.3 [e]
The present study (classical PSHA on bedrock, 475 years)	DMR	Yes	Yes	Yes	Yes	Yes	0.14–0.19	
The present study (classical PSHA on surface, 475 years)	DMR	Yes	Yes	Yes	Yes	Yes	0.18–0.41	

(a) Seismic hazard analysis at the bedrock

(b) By considering measured V_{S30} values

(c) By applying Abrahamson & Silva (1997) GMPE

(d) By applying Islam et al. (2010) GMPE

(e) Scenario-based PGA for Madhupur Fault (Mw: 7.5)

the site effect and use the PGA and design spectra of the surface for further analysis and urban development planning.

Declarations

Conflict of interests The authors have not disclosed any competing interests.

References

Abrahamson NA, Silva WJ (1997) Empirical response spectral attenuation relations for shallow crustal earthquakes. Seismol Res Lett 68:94–127

Abrahamson N, Silva W (2008) Summary of the Abrahamson & Silva NGA ground-motion relations. Earthq Spectra 24:67–97. https://doi.org/10.1193/1.2924360

Akkar S, Bommer JJ (2010) Empirical equations for the prediction of PGA, PGV, and spectral accelerations in Europe, the Mediterranean Region, and the Middle East. Seismol Res Lett 81:195–206. https://doi.org/10.1785/GSSRL.81.2.195

al Atik L, Abrahamson N, (2010) An improved method for nonstationary spectral matching. Earthq Spectra 26:601–617

Alam E, Dominey-Howes D (2016) A catalogue of earthquakes between 810BC and 2012 for the Bay of Bengal. Nat Hazards 81:2031–2102

Alam M, Alam MM, Curray JR et al (2003) An overview of the sedimentary geology of the Bengal Basin in relation to the regional tectonic framework and basin-fill history. Sediment Geol 155:179–208

Al-Hussaini TM, Al-Noman MN (2010) Probabilistic estimates of PGA and Spectral Acceleration in Bangladesh. In: Proceedings, 3rd international earthquake symposium, Bangladesh, Dhaka. pp 5–6

Al-Hussaini TM, Chowdhury IN, Noman MN (2015) Seismic hazard assessment for Bangladesh-old and new perspectives. In: First International Conference on Advances in Civil Infrastructure and Construction Materials. Military Institute of Science & Technology, pp 841–856

Ambraseys NN, Douglas J (2004) Magnitude calibration of north Indian earthquakes. Geophys J Int 159:165–206

Ambraseys NN, Jackson JA (1998) Faulting associated with historical and recent earthquakes in the Eastern Mediterranean region. Geophys J Int 133:390–406

Ansal A, Tönük G, Kurtuluş A (2018) Implications of site specific response analysis. In: European Conference on Earthquake Engineering Thessaloniki, Greece. Springer, pp 51–68

ASCE (2017) Minimum design loads and associated criteria for buildings and other structures. American Society of Civil Engineers

Ashish LC, Parvez IA, Kühn D (2016) Probabilistic earthquake hazard assessment for Peninsular India. J Seismol 20:629–653. https://doi.org/10.1007/s10950-015-9548-2

Atkinson GM, Boore DM (1995) Ground-motion relations for eastern North America. Bull Seismol Soc Am 85:17–30. https://doi.org/10.1785/BSSA0850010017

Atkinson GM, Boore DM (2003) Empirical ground-motion relations for subduction-zone earthquakes and their application to Cascadia and other regions. Bull Seismol Soc Am 93:1703–1729. https://doi.org/10.1785/0120020156

Atkinson GM, Boore DM (2006) Earthquake ground-motion prediction equations for eastern North America. Bull Seismol Soc Am 96:2181–2205

Atkinson GM, Boore DM (2011) Modifications to existing ground-motion prediction equations in light of new data. Bull Seismol Soc Am 101:1121–1135. https://doi.org/10.1785/0120100270

Bendimerad F, Morrow GC (2014) Dhaka earthquake risk guidebook Bangladesh urban Earthquake resilience project

Bhatia SC, Kumar MR, Gupta HK (1999) A probabilistic seismic hazard map of India and adjoining regions

Blaser L, Krüger F, Ohrnberger M, Scherbaum F (2010) Scaling relations of earthquake source parameter estimates with special focus on subduction environment. Bull Seismol Soc Am 100:2914–2926

Boncio P, Lavecchia G, Pace B (2004) Defining a model of 3D seismogenic sources for Seismic Hazard Assessment applications: The case of central Apennines (Italy). J Seismol 8:407–425. https://doi.org/10.1023/B:JOSE.0000038449.78801.05

Boore DM, Atkinson GM (2008) Ground-motion prediction equations for the average horizontal component of PGA, PGV, and 5%-damped PSA at spectral periods between 0.01 s and 10.0 s. Earthq Spectra 24:99–138. https://doi.org/10.1193/1.2830434

Boore DM, Joyner WB, Fumal TE (1997a) Equations for estimating horizontal response spectra and peak acceleration from Western North American earthquakes: a summary of recent work. Seismol Res Lett 68:128–153. https://doi.org/10.1785/GSSRL.68.1.128

Campbell KW (2003) Prediction of strong ground motion using the hybrid empirical method and its use in the development of ground-motion (attenuation) relations in eastern North America. Bull Seismol Soc Am 93:1012–1033

Campbell KW, Bozorgnia Y (2003) Updated Near-Source Ground-Motion (Attenuation) Relations for the Horizontal and Vertical Components of Peak Ground Acceleration and Acceleration Response Spectra. Bull Seismol Soc Am 93:314–331. https://doi.org/10.1785/0120020029

Campbell KW, Bozorgnia Y (2008) NGA ground motion model for the geometric mean horizontal component of PGA, PGV, PGD and 5% damped linear elastic response spectra for periods ranging from 0.01 to 10 s. Earthq Spectra 24:139–171

Campbell KW, Bozorgnia Y (2007) Campbell-Bozorgnia NGA ground motion relations for the geometric mean horizontal component of peak and spectral ground motion parameters. Pacific Earthquake Engineering Research Center

Chaulagain H, Rodrigues H, Silva V et al (2015) Seismic risk assessment and hazard mapping in Nepal. Nat Hazards 78:583–602. https://doi.org/10.1007/s11069-015-1734-6

Chiou BJ, Youngs RR (2008) An NGA model for the average horizontal component of peak ground motion and response spectra. Earthq Spectra 24(1):173–215

Chiou BS-J, Youngs RR (2014) Update of the Chiou and Youngs NGA model for the average horizontal component of peak ground motion and response spectra. Earthq Spectra 30:1117–1153

Das R, Wason HR, Sharma ML (2011) Global regression relations for conversion of surface wave and body wave magnitudes to moment magnitude. Nat Hazards 59:801–810

Du W, Pan T-C (2020) Probabilistic seismic hazard assessment for Singapore. Nat Hazards 103:2883–2903. https://doi.org/10.1007/s11069-020-04107-4

Engdahl ER, van der Hilst R, Buland R (1998) Global teleseismic earthquake relocation with improved travel times and procedures for depth determination. Bull Seismol Soc Am 88:722–743

Frankel A (1995) Mapping seismic hazard in the central and eastern United States. Seismol Res Lett 66:8–21

Gahalaut VK, Kundu B (2012) Possible influence of subducting ridges on the Himalayan arc and on the ruptures of great and major Himalayan earthquakes. Gondwana Res 21:1080–1088

Gardner JK, Knopoff L (1974) Is the sequence of earthquakes in Southern California, with aftershocks removed, Poissonian? Bull Seismol Soc Am 64:1363–1367

Ghasemi Nejad R, Ali Abbaspour R, Mojarab M (2021) Associating earthquakes with faults using cluster analysis optimized by a fuzzy particle swarm optimization algorithm for Iranian provinces. Soil Dyn Earthq Eng 140:106433. https://doi.org/10.1016/j.soildyn.2020.106433

Gupta ID (2006) Delineation of probable seismic sources in India and neighbourhood by a comprehensive analysis of seismotectonic characteristics of the region. Soil Dyn Earthq Eng 26:766–790. https://doi.org/10.1016/J.SOILDYN.2005.12.007

Gutenberg B, Richter CF (1944) Frequency of earthquakes in California. Bull Seismol Soc Am 34:185–188

Haque DME, Khan NW, Selim M, et al (2019) Towards improved probabilistic seismic hazard assessment for Bangladesh. Pure Appl Geophys 1–30

Hurukawa N, Tun PP, Shibazaki B (2012) Detailed geometry of the subducting Indian Plate beneath the Burma Plate and subcrustal seismicity in the Burma Plate derived from joint hypocenter relocation. Earth, Planets and Space 64:333–343

Iervolino I, Cornell CA (2005) Record selection for nonlinear seismic analysis of structures. Earthq Spectra 21:685–713

Islam MS, Shinjo R (2012) The Dauki fault at the Shillong plateau-bengal basin boundary in northeastern India: 2D finite element modeling. Journal of Earth Science 23:854–863

Islam ABMS, Jameel M, Uddin MA, Ahmad SI (2011) Simplified design guidelines for seismic base isolation in multi-storey buildings for Bangladesh National Building Code (BNBC). International Journal of Physical Sciences 6:5467–5486

Jackson J (2001) Living with earthquakes: know your faults. J Earthquake Eng 5:5–123

Jia J, Jia (2018) Soil dynamics and foundation modeling. Springer

Jia J (2016) Modern earthquake engineering: Offshore and land-based structures. Springer

Kaklamanos J, Baise LG, Boore DM (2011) Estimating unknown input parameters when implementing the NGA ground-motion prediction equations in engineering practice. Earthq Spectra 27:1219–1235

Kamal A. SMM (2013) Earthquake risk and reduction approaches in bangladesh. in: shaw r, mallick f, islam a (eds) disaster risk reduction approaches in Bangladesh. Springer Japan, Tokyo, pp 103–130

Kayal JR (2008a) Microearthquake seismology and seismotectonics of South Asia. Springer Science & Business Media

Kayal JR (2008b) Northeast India, Myanmar, Bangladesh and Andaman-Sumatra region. microearthquake seismology and seismotectonics of South Asia 266–347

Kijko A (2004) Estimation of the maximum earthquake magnitude, m max. Pure Appl Geophys 161:1655–1681

Kijko A, Sellevoll MA (1992) Estimation of earthquake hazard parameters from incomplete data files. Part II. Incorporation of magnitude heterogeneity. Bull Seismol Soc Am 82:120–134

Kolathayar S, Sitharam TG, Vipin KS (2012) Deterministic seismic hazard macrozonation of India. J Earth Syst Sci 121:1351–1364

Kumar P, Yuan X, Kumar MR et al (2007) The rapid drift of the Indian tectonic plate. Nature 449:894–897

Lin PS, Lee CT (2008) Ground-motion attenuation relationships for subduction-zone earthquakes in Northeastern Taiwan. Bull Seismol Soc Am 98:220–240. https://doi.org/10.1785/0120060002

Mallick R, Lindsey EO, Feng L et al (2019) Active convergence of the India-Burma-Sunda plates revealed by a new continuous GPS network. J Geophys Res Solid Earth 124:3155–3171

Martin S, Szeliga W (2010) A catalog of felt intensity data for 570 earthquakes in India from 1636 to 2009. Bull Seismol Soc Am 100:562–569

Mase LZ, Farid M, Sugianto N (2021) Seismic hazard vulnerability based on probabilistic seismic hazard approach in Bengkulu City. Indonesia. AIP Conf Proc 2320:040020. https://doi.org/10.1063/5.0037550

McGuire JJ (2004) Estimating finite source properties of small earthquake ruptures. Bull Seismol Soc Am 94:377–393

Ministry of Housing & Public Works (1993) Bangladesh National Building Code (BNBC)

Ministry of Housing & Public Works (2020) Bangladesh National Building Code (BNBC)

Mohajer-Ashjai A, Nowroozi AA (1978) Observed and probable intensity zoning of Iran. Tectonophysics 49:149–160. https://doi.org/10.1016/0040-1951(78)90173-7

Morino M, Kamal ASMM, Akhter SH et al (2014) A paleo-seismological study of the Dauki fault at Jaflong, Sylhet, Bangladesh: Historical seismic events and an attempted rupture segmentation model. J Asian Earth Sci 91:218–226

Nath SK, Thingbaijam KKS (2012) Probabilistic seismic hazard assessment of India. Seismol Res Lett 83:135–149

Nath SK, Thingbaijam KKS, Maiti SK, Nayak A (2012) Ground-motion predictions in Shillong region, northeast India. J Seismol 16:475–488. https://doi.org/10.1007/S10950-012-9285-8/METRICS

Nath SK, Mandal S, Adhikari M, das, Maiti SK, (2017a) A unified earthquake catalogue for South Asia covering the period 1900–2014. Nat Hazards 85:1787–1810

Nath SK, Mandal S, Das Adhikari M, Maiti SK (2017b) A unified earthquake catalogue for South Asia covering the period 1900–2014. Nat Hazards 85:1787–1810. https://doi.org/10.1007/s11069-016-2665-6

Ouillon G, Ducorbier C, Sornette D (2008) Automatic reconstruction of fault networks from seismicity catalogs: Three-dimensional optimal anisotropic dynamic clustering. J Geophys Res Solid Earth. https://doi.org/10.1029/2007JB005032

Pagani M, Monelli D, Weatherill G et al (2014) OpenQuake engine: an open hazard (and risk) software for the global earthquake model. Seismol Res Lett 85:692–702

Pagani M, Garcia-Pelaez J, Gee R, et al (2018) Global Earthquake Model (GEM) Seismic Hazard Map (version 2018.1–December 2018), DOI: 10.13117. GEM-GLOBAL-SEISMIC-HAZARD-MAP-2018.1

Pandey AK, Chingtham P, Roy PNS (2017) Homogeneous earthquake catalogue for Northeast region of India using robust statistical approaches. Geomat Nat Haz Risk 8:1477–1491

Pezeshk S, Zandieh A, Tavakoli B (2011) Hybrid empirical ground-motion prediction equations for Eastern North America using NGA Models and updated seismological parameters. Bull Seismol Soc Am 101:1859–1870. https://doi.org/10.1785/0120100144

Phillips WS, Aki K (1986) Site amplification of coda waves from local earthquakes in central California. Bull Seismol Soc Am 76:627–648

Pitilakis K (2004) Site effects. In: Recent advances in earthquake geotechnical engineering and microzonation. Springer, pp 139–197

Qodri MF, Mase LZ, Likitlersuang S (2021) Non-linear site response analysis of Bangkok subsoils due to earthquakes triggered by three pagodas fault. Eng J 25:43–52. https://doi.org/10.4186/ej.2021.25.1.43

Raghu Kanth STG, Iyengar RN (2007) Estimation of seismic spectral acceleration in peninsular India. J Earth Syst Sci 116:199–214

Rahman M, Siddiqua S, Kamal ASM (2020) Seismic source modeling and probabilistic seismic hazard analysis for Bangladesh. Nat Hazards 103:2489–2532

Rajendran CP, Rajendran K, Duarah BP, et al (2004) Interpreting the style of faulting and paleoseismicity associated with the 1897 Shillong, northeast India, earthquake: Implications for regional tectonism. Tectonics 23:

Raoof J, Mukhopadhyay S, Koulakov I, Kayal JR (2017) 3-D seismic tomography of the lithosphere and its geodynamic implications beneath the northeast India region. Tectonics 36:962–980

Rathje EM, Kottke AR, Trent WL (2010) Influence of input motion and site property variabilities on seismic site response analysis. J Geotech Geoenviron Eng 136:607–619

Rydelek PA, Sacks IS (1989) Testing the completeness of earthquake catalogues and the hypothesis of self-similarity. Nature 337:251–253

Sarker JK, Ansary MA, Rahman MS, Safiullah AMM (2010) Seismic hazard assessment for Mymensingh, Bangladesh. Environ Earth Sci 60:643–653. https://doi.org/10.1007/S12665-009-0204-4/METRICS

Satyabala S (2003) Oblique plate convergence in the Indo-Burma (Myanmar) subduction region. Pure Appl Geophys 160:1611–1650

Scordilis EM (2006) Empirical global relations converting MS and MB to moment magnitude. J Seismol 10:225–236

B. SH (1970) Soil moduli and damping factors for dynamic response analyses. Reoprt EERC 70–10

Sharma ML, Douglas J, Bungum H, Kotadia J (2009) Ground-motion prediction equations based on data from the Himalayan and Zagros regions. J Earthquake Eng 13:1191–1210

Sitharam TG, James N, Kolathayar S (2018) Comprehensive seismic zonation schemes for regions at different scales. Springer

Socquet A, Vigny C, Chamot-Rooke N et al (2006) India and Sunda plates motion and deformation along their boundary in Myanmar determined by GPS. J Geophys Res Solid Earth 111:B5

Spence W (1989) Stress origins and earthquake potentials in Cascadia. J Geophys Res Solid Earth 94:3076–3088

Stewart JP, Liu AH, Choi Y (2003) Amplification factors for spectral acceleration in tectonically active regions. Bull Seismol Soc Am 93:332–352

Stork AL, Selby ND, Heyburn R, Searle MP (2008) Accurate relative earthquake hypocenters reveal structure of the Burma subduction zone. Bull Seismol Soc Am 98:2815–2827

Strasser FO, Arango MC, Bommer JJ (2010) Scaling of the source dimensions of interface and intraslab subduction-zone earthquakes with moment magnitude. Seismol Res Lett 81:941–950

Szeliga W, Hough S, Martin S, Bilham R (2010) Intensity, magnitude, location, and attenuation in India for felt earthquakes since 1762. Bull Seismol Soc Am 100:570–584

Tavakoli B, Pezeshk S (2005) Empirical-stochastic ground-motion prediction for eastern North America. Bull Seismol Soc Am 95:2283–2296

Toro GR (2002) Modification of the Toro et al.(1997) attenuation equations for large magnitudes and short distances. Risk Engineering Technical Report

Valdiya KS (1984) Evolution of the Himalaya. Tectonophy. https://doi.org/10.1016/0040-1951(84)90205-1

van Stiphout T, Zhuang J, Marsan D (2012) Seismicity declustering. Commun Online Resfor Stat Seismicity Anal 10:1–25

Villar-Vega M, Silva V, Crowley H et al (2017) Development of a fragility model for the residential building stock in South America. Earthq Spectra 33:581–604

Vucetic M, Dobry R (1991) Effect of Soil Plasticity on Cyclic Response. J Geotech Eng 117:89–107. https://doi.org/10.1061/(ASCE)0733-9410(1991)117:1(89)

Wells DL, Coppersmith KJ (1994) New empirical relationships among magnitude, rupture length, rupture width, rupture area, and surface displacement. Bull Seismol Soc Am 84:974–1002

Wiemer S, Wyss M (2000) Minimum magnitude of completeness in earthquake catalogs: Examples from Alaska, the western United States, and Japan. Bull Seismol Soc Am 90:859–869

Yadav RBS, Tripathi JN, Rastogi BK et al (2010) Probabilistic assessment of earthquake recurrence in northeast India and adjoining regions. Pure Appl Geophys 167:1331–1342

Yilmaz C, Silva V, Weatherill G (2021) Probabilistic framework for regional loss assessment due to earthquake-induced liquefaction including epistemic uncertainty. Soil Dynam Earthq Eng 141:106493. https://doi.org/10.1016/J.SOILDYN.2020.106493

Youngs RR, Chiou SJ, Silva WJ, Humphrey JR (1997) Strong Ground Motion Attenuation Relationships for Subduction Zone Earthquakes. Seismol Res Lett 68:58–73. https://doi.org/10.1785/GSSRL.68.1.58

Zhang P, Yang Z, Gupta HK, et al (1999) Global seismic hazard assessment program (GSHAP) in continental Asia

Zhao JX, Zhang J, Asano A et al (2006) Attenuation relations of strong ground motion in Japan using site classification based on predominant period. Bull Seismol Soc Am 96:898–913. https://doi.org/10.1785/0120050122

Zhao JX, Jiang F, Shi P et al (2016) Ground-motion prediction equations for subduction slab earthquakes in Japan using site class and simple geometric attenuation functions. Bull Seismol Soc Am 106:1535–1551. https://doi.org/10.1785/0120150056

Zimmaro P, Stewart JP (2017) Site-specific seismic hazard analysis for Calabrian dam site using regionally customized seismic source and ground motion models. Soil Dyn Earthq Eng 94:179–192. https://doi.org/10.1016/J.SOILDYN.2017.01.014